Sarbecovirus Rc-o319 S-Protein Structures Reveal Highly Specialized Adaptation to *Rhinolophus cornutus* ACE2

Jingjing Wang[1,2,†], Zexuan Li[1,3,†], Yong Ma[1,2,†], Zimu Li[1,4,5], Hang Yuan[1,3], Chuanying Niu[1,6], Banghui Liu[1,2], Mei Li[4], Min Zhou[4], Wenxiu Liu[4], Huimin Feng[1], Jing Chen[4], Jun He[1,2], Xinwen Chen[4,*], Xiaoli Xiong[1,2,*]

1 State Key Laboratory of Respiratory Disease, Guangdong Provincial Key Laboratory of Stem Cell and Regenerative Medicine, Guangdong-Hong Kong Joint Laboratory for Stem Cell and Regenerative Medicine, Guangzhou Institutes of Biomedicine and Health, Chinese Academy of Sciences, Guangzhou 510530, China.

2 Graduate School of Guangzhou Medical University, Guangzhou Medical University-Guangzhou Institutes of Biomedicine and Health Joint School of Life Sciences, Guangzhou Medical University, Guangzhou 511436, China.

3 University of Chinese Academy of Sciences, Beijing 100864, China.

4 Guangzhou National Laboratory, Guangzhou 510005, China.

5 Guangzhou Medical University, Guangzhou 511436, China.

6 University of Science and Technology of China, Hefei 230026, Anhui, China

†These authors contributed equally to this work.

*Corresponding author. Email: chen_xinwen@gzlab.ac.cn (X.C.); xiong_xiaoli@gibh.ac.cn (X.X.)

Abstract

Sarbecoviruses, represented by SARS-CoV-1 and SARS-CoV-2, utilize their spike (S) proteins to bind host ACE2 receptors and initiate infection. Here, we characterize the S-protein of Rc-o319, a sarbecovirus identified in Japanese *Rhinolophus cornutus* bats, which exhibits highly restricted receptor specificity. Functional assays demonstrate that Rc-o319 S-protein preferentially utilizes its cognate *R. cornutus* ACE2 (bACE2$_{R.cor}$). Cryo-EM structures reveal two locked prefusion conformations of the Rc-o319 S-trimer and identify a novel Type-4 receptor-binding domain (RBD), featuring a distinct beta-loop (BL) element within the receptor-binding motif (RBM). The Rc-o319-RBD:bACE2$_{R.cor}$ complex structure reveals unique contact features, including specialized BL mediates interactions with bACE2$_{R.cor}$ and interactions mediated a bACE2$_{R.cor}$ glycan. Structure-guided mutagenesis demonstrates that the BL-RBM-loop co-adaptation within the Rc-o319 S-protein poses a barrier to hACE2 utilization. Comparative assays further show that the bACE2$_{R.cor}$ receptor supports only a subset of sarbecoviruses, highlighting its restricted sarbecovirus compatibility. Our findings establish the Rc-o319 S-protein as a structurally and functionally specialized adaptation to *R. cornutus* ACE2 and underscore the structural constraints limiting its cross-species transmission potential.

Introduction

The SARS-CoV-1 (also known as SARS-CoV) outbreak(Drosten et al., 2003, Fouchier et al., 2003, Peiris et al., 2003, Peiris et al., 2004) and the SARS-CoV-2 pandemic have profoundly impacted global public health. Surveillance efforts have since detected multiple SARS-related coronaviruses (SARSr-CoVs) primarily in horseshoe bats (genus *Rhinolophus*) worldwide(Drexler et al., 2010, Murakami et al., 2020, Tao & Tong, 2019, Temmam et al., 2022, Wacharapluesadee et al., 2021), suggesting they are the likely natural reservoir for SARSr-CoVs (Ge et al., 2013, Hu et al., 2015, Li et al., 2005b). Along with SARS-CoV-1 and SARS-CoV-2, SARSr-CoVs have been classified into the *Sarbecovirus* subgenus in the *Betacoronavirus* family (https://ictv.global/taxonomy). Sarbecoviruses share considerable similarity in their spike (S) proteins with amino-acid (AA) sequence identity > 63% (Alkhovsky et al., 2022, Delaune et al., 2021, Guo et al., 2023, Wang et al., 2025, Wells et al., 2021, Zhou et al., 2021). Like other coronaviruses (CoVs), sarbecovirus S-protein assembles into a large, glycosylated homo-trimer on the virion surface. Each S-protein protomer can be divided into two parts: the S1 part, responsible for cell attachment, and the S2 part, facilitating virus-cell membrane fusion (Bosch et al., 2003, Harrison, 2008, Zhang et al., 2021a). For a sarbecovirus S-protein, its S1 parts can be further divided as the N-terminal domain (NTD), receptor binding domain (RBD), Domain C (also called subdomain-1, SD-1) and Domain D (also called subdomain-2, SD-2) (Gui et al., 2017, Song et al., 2018, Wang et al., 2025, Xiong et al., 2020, Zhang et al., 2021a, Zhang et al., 2023). The S-RBD can be further divided into a core domain, onto which a receptor binding motif (RBM) region is attached (Li et al., 2005a, Wang et al., 2025). The RBM primarily contacts the receptor, forming the interaction interface with the receptor (Li et al., 2005a, Si et al., 2024, Song et al., 2018, Yan et al., 2020).

For both SARS-CoV-1 (Li et al., 2005a, Li et al., 2005c) and SARS-CoV-2 (Han et al., 2021, Zhou et al., 2020a) their S-RBDs bind with the human ACE2 (hACE) receptor with high affinities in the nano-molar range, suggesting that high-affinity hACE2 binding is likely a key prerequisite for spill-over into the human population.

Of note, not all bat SARSr-CoVs can bind hACE2 with high-affinity (Alkhovsky et al., 2022, Crook et al., 2021, Delaune et al., 2021, Guo et al., 2023, Hu et al., 2015, Markotter et al., 2019, Murakami et al., 2020, Temmam et al., 2022, Zhou et al., 2021). We previously reported that sarbecovirus S-protein can be classified into three types based on their RBM structural features. Four featured RBM regions have been defined, namely the large-loop (LL), lamella (LM), small-loop (SL), and finally the anchor-loop (AL) (Wang et al., 2025). Type-1 S-proteins, including SARS-CoV-1, SARS-CoV-2 and WIV1, possess intact LL and SL regions. Type-1 S-proteins often bind hACE2, albeit with varying affinities: SARS-CoV-1 and SARS-CoV-2 bind hACE2 with high affinities, whereas WIV1 binds hACE2 with a moderate affinity. We found high-affinity hACE2 binding requires synergistic favourable hACE2 interactions across the four featured RBM regions. Type-2 S-proteins, including BM48-31 and BtKY72, have an intact LL but a deleted SL. They generally lack hACE binding but can bind selected bat ACE2 (bACE2) orthologs with intermediate affinities. Type-3 S-proteins, including HeB2013 and RmYN02, have both their LL and SL regions deleted. They have yet been reported to bind neither hACE2 nor bACE2.

Ongoing surveillance in Japan has recently discovered several new SARSr-CoVs in the little Japanese horseshoe bat - *Rhinolophus cornutus* (*R.cor*) detected in 2020 using samples collected in 2013 (Murakami et al., 2020). The presentative virus, Rc-o319, is distantly related to SARS-CoV-2, sharing 81% whole-genome identity. Importantly, although its S-protein has 81% AA identity to SARS-CoV-2 S-protein, its RBM contains a unique nine-amino-acid deletion relative to SARS-CoV-2 that removes residues identified critical for ACE2 binding in other SARSr-CoVs and likely alters its RBM structure (Murakami et al., 2020). Deletions in the RBMs of SARSr-CoVs have been shown to greatly affect ACE2 binding (Hu et al., 2022, Si et al., 2024). In this study, we surveyed binding of Rc-o319 S-protein to various ACE2 orthologs to understand its specificity. Further, we determined the structures of the Rc-o319 S-trimers and of the Rc-o319-RBD bound to *R. cornutus* ACE2 ($bACE2_{R.cor}$), thereby establishing the Rc-o319 RBD as a novel Type-4 RBD. By analysing the molecular determinants of receptor specificity revealed by our structures, we identify the changes necessary to switch the specificity of the Rc-o319 S-protein to hACE2. These findings provide insights into Rc-o319's

adaptations to various ACE2 orthologs and provide an assessment of its cross-species transmission potential.

Results

Rc-o319 S utilizes a narrow range of *Rhinolophus* bat ACE2 orthologs as receptors

We used a S:ACE2 interaction mediated cell-cell fusion assay to identify ACE2 orthologs that can interact with Rc-o319-S-protein (Ma et al., 2023). Effector cells expressing Rc-o319 S-proteins were tested against receptor cells expressing a panel of ACE2 orthologs for fusion activity (**Fig. 1A**). In this assay, several *Rhinolophus affinis* (*Ra*) and *Rhinolophus sinicus* (*Rs*) ACE2 molecules, including *Ra*5538, *Ra*9479, *Rs*1446, *Rs*3359, and *Rs*3366, were found to mediate varying levels of cell-cell fusion, with *Ra*9479 showing the highest activity and *Rs*3366 the lowest. However, all were substantially weaker than the cognate bACE2$_{R.cor}$ receptor. Rc-o319 S-protein is unable to utilize pangolin and human ACE2 (hACE2) orthologs for fusion. Receptor binding assays using biolayer interferometry (BLI) show that Rc-o319-RBD-Fc and Rc-o319-S-trimer bind bACE2$_{R.cor}$ with moderate-to-high affinities (**Fig.1B** left panels, 76 nM for RBD-Fc and 27 nM for S-trimer**)**. Although Rc-o319 appears to somewhat use bACE2$_{Ra9479}$, showing weak fusion activity in the cell-cell fusion assay. BLI assays were unable to detect bACE2$_{Ra9479}$ binding by the Rc-o319 S-trimer and dimeric Rc-o319-RBD-Fc **(Fig.1B**, middle panels**)**. Rc-o319-S-trimer binds bACE2$_{R.cor}$ with relative weak responses and an estimated affinity of 27 nM, tighter than that observed for the dimeric Rc-o319-RBD-Fc, indicating avidity-amplified receptor binding (**Fig.1B,** left panels). Consistent with the cell-cell fusion assay results, neither Rc-o319-RBD-Fc nor Rc-o319-S-trimer is able to bind hACE2 (**Fig.1B**, right panels**)**. These results demonstrate that Rc-o319-S-protein has a restricted ACE2 specificity, with a clear preference towards its cognate bACE2$_{R.cor}$ receptor (**Fig.1A** and **B)**.

Structures of the Rc-o319 S-protein identify a new type of RBM

To understand the unusual restricted receptor specificity of Rc-o319 S-protein, purified Rc-o319 S-protein ectodomain was imaged by cryo-electron microscopy (Cryo-EM) (**Figs. 1**), revealing that Rc-o319 S-trimers adopt two distinct conformations (**Fig. 1D-I, Figs. 1, Figs. 2** and **Figs. 3A**). In both conformations, the 3 RBDs in each S-trimer are all in “down” positions (**Fig. 1D** and **G**). Detailed

structural analysis reveals tight trimer packing for both conformations and based on their structural features, the two conformations have been identified as “locked-1” and “locked-2” conformations previously identified for both SARS-CoV-1 and SARS-CoV-2 S-trimers (Cai et al., 2020, Ke et al., 2020, Qu et al., 2022, Xiong et al., 2020, Zhang et al., 2023) (**Figs. 2**).

In the locked-1 Rc-o319 S-trimer, each RBD contains a density that can be modelled as a fatty acid with 18-carbon atoms, previous mass-spectrometry analysis identified it being either linoleic acid (Toelzer et al., 2020, Zhang et al., 2021b) or oleic acid (Ma et al., 2021) (**Fig. 1E** and **Figs. 3C**). Consistent with previous observations, the aliphatic tail of the fatty acid is bound within the hydrophobic fatty-acid binding pocket of one RBD, while its carboxylate group forms salt-bridges with $R382_{Rc\text{-}o319}$ of a neighbouring RBD (**Fig. 1E and Figs. 3C**); these fatty acid mediated inter-protomer interactions likely stabilise the S-trimer in the observed locked conformation. Each NTD also contains a density corresponding to a biliverdin molecule. Binding of biliverdin has been correlated with evasion of antibody immunity (Freeman et al., 2023, Rosa et al., 2021) (**Fig. 1D** and **1G** and **Figs. 3D**). Consistent with being in a locked conformation, the fusion peptide proximal region (FPPR) is ordered (**Fig. 1F**). Finally, consistent with the locked-1 conformation observed for the S-proteins of SARS-CoV-1 (Zhang et al., 2023) and SARS-CoV-2 (Qu et al., 2022), residues $580\text{-}605_{Rc\text{-}o319}$ form a large disordered loop within Domain D of the Rc-o319 S-trimer (**Fig. 1D** and **F**).

In the locked-2 conformation, no fatty acid density was observed within the RBD fatty-acid binding pocket (**Fig. 1H**). This is accompanied with a restructuring of the fatty-acid binding pocket (**Fig. 1H** and **Figs. 3C**) as observed when the fatty-acid binding pockets were vacated in other sarbecovirus S-trimers (Lee et al., 2023, Toelzer et al., 2020). Each NTD still contains a density corresponds to a biliverdin (**Fig. 1D** and **1G**). The FPPR is ordered (**Fig. 1I**). Differently, the disordered Domain D loop in the locked-1 conformation refolds and forms a large ordered loop structure, packing against the core of the Domain D and the junction between Domains C and D (**Fig. 1F**) (Qu et al., 2022, Zhang et al., 2023).

A structural change between locked-1 and locked-2 conformations in the Domain C-D junction region can be observed similar to previous observations on the S-proteins of SARS-CoV-1 and SARS-CoV-2 (Qu et al., 2022, Zhang et al., 2023) (**Figs. 3A**). Near the 3-fold axis, to the top of the S-trimer, $D468_{Rc\text{-}o319}$ forms an intra-protomer hydrogen bond with $Y473_{Rc\text{-}o319}$ in the locked-1 conformation (**Fig. 2A**). Whereas in locked-2 conformation, $D468_{Rc\text{-}o319}$ mediates two inter-protomer hydrogen bonds with $S469_{Rc\text{-}o319}$ of a neighbouring S-protomer (**Fig. 2B**). Of Note, in both conformations, $K458_{Rc\text{-}o319}$, equivalent to $Q493_{SARS2}$, previously identified as an important determinant for ACE2 specificity (Dadonaite et al., 2024, Li, 2008, Wang et al., 2025), is found to form an inter-protomer hydrogen bond to the glycan attaching to $N344_{Rc\text{-}o319}$ of a neighbouring S-protomer (**Fig. 2A-B**). Inter-molecular hydrogen bonds likely affect S-trimer stability.

In both Rc-o319 S-trimer conformations, their NTDs are well resolved, revealing five loops that are markedly shorter than those in SARS-CoV-2 (**Fig. 2C-D** and **Figs. 3E**). In addition, a four-amino-acid insertion (residues $189\text{-}192_{Rc\text{-}o319}$) is identified in the Rc-o319 NTD, forming an “inserted loop” exposed to the exterior of the trimer (**Figs. 3B**). Because the NTD is under strong immune pressure (Harvey et al., 2021, McCallum et al., 2021), these truncated and elongated loops likely endow the NTD of Rc-o319 S-protein with a distinct antigenic profile.

Finally, Rc-o319 S-trimer structures show that their RBDs form structures distinct from previous characterized sarbecovirus RBDs (**Fig. 2E-G** and **Figs. 4**). In contrast to Type-3 RBDs, where 13- to 14-amino-acid deletions relative to SARS-CoV-2 eliminate the large-loop (LL) (**Figs. 4F-G**), the Rc-o319 RBD retains an extension in a similar region as the LL of Type-1 RBDs, despite a nine-amino-acid deletion (**Fig. 2E**). In the Type-1 RBD, the LL is formed by two half-loops stabilized by an intra-loop disulfide bond (**Fig. 2F**). By contrast, the equivalent extension in the Rc-o319 RBD comprises two small antiparallel β-sheets connected by a short loop (**Fig. 2E** and **Fig. 3**). We designate this distinct extension a beta-loop (BL) structure. Due to the nine-amino-acid deletion, the stabilizing disulfide

bond found in the LL is lost.The shorter BL occupies a position roughly corresponding to the C-terminal half-loop of the LL in Type-1 RBDs (**Fig. 2E-G** and **Fig. 3D)**, albeit with notable conformational and tilting angle differences (**Fig. 2G,** also see **Fig. 3D**). This distinct beta-loop (BL) structure, by comparison with the LL structure in Type-1 RBDs (**Fig. 2F**), suggests that the Rc-o319-RBD likely binds ACE2 with distinct interactions.

Structure of the Rc-o319-RBD:bACE2$_{R.cor}$ complex

To further understand the receptor binding by the Rc-o319 S-protein, we determined a structure of Rc-o319-RBD in complex with its cognate bACE2$_{R.cor}$ receptor (**Fig. 3** and **Figs. 1B**). The structure reveals that Rc-o319-RBD and bACE2$_{R.cor}$ bind with each other using similar molecular surfaces previous observed in other sarbecovirus RBD:ACE2 complexes (**Fig. 3A-B**). However, distinctively, a glycan linked to Asn38 of bACE2$_{R.cor}$ is involved in the binding interface (**Fig. 3A, E** and **H-I**) (interfacial residues in the RBD and ACE2 are denoted using single-letter and three-letter amino acid codes, respectively). The BSA of the complex was calculated as 1005 Å^2, which includes a contribution of 252 Å^2 from the binding of the Asn38-linked glycan. In line with previous interface analysis, the binding interface can be divided into the beta-loop (BL), lamella (LM), anchor loop (AL) and small loop (SL) regions (**Fig. 3F-I)**.

The beta-loop (BL) of Rc-o319 RBD engages highly distinctive interactions (**Fig. 3A** and **F**). Due to its distinct structure and protrusion from the RBM, the BL contacts the bACE2$_{R.cor}$ near Lys27, forming a hydrogen bond with side chain of Lys27 (**Fig. 3A** and **F**). In contrast, LL in Type-1 RBDs contacts ACE2 near residue 24, more towards the ACE2 N-terminus (**Fig. 3J**). Distinctively, BL residue Y447$_{\text{Rc-o319}}$ forms a charged hydrogen bond with Asp31 of bACE2$_{R.cor}$ (**Fig. 3A** and **F**). Of note, the positively charged residue K454$_{\text{Rc-o319}}$, unique to the Rc-o319 RBM, extends from the BL to form a salt-bridge with Glu75$_{\text{Rc-o319}}$ of bACE2$_{R.cor}$ (**Fig. 3A**) and is positioned in close proximity to the negatively charged bACE2$_{R.cor}$ residues Asp31 and Glu35 (**Fig. 3F-G**). Changing this residue K454Y$_{\text{Rc-o319}}$ to the corresponding residue Y in SARS-CoV-2 substantially reduced

bACE2$_{R.cor}$ binding **(Figs. 8B**). Also distinctively, the large RBM-loop (**Fig. 2E, 3C, 3F** and **Figs. 6**) structure N-terminal to the BL is involved in Rc-o319 ACE2 binding (**Fig. 3F**). W430$_{Rc\text{-}o319}$ in the RBM-loop forms a cation-π interaction with Lys27, and likely stabilizes the BL, forming a π-π interaction with the BL residue Y447$_{Rc\text{-}o319}$ (**Fig. 3F**).

In the lamella (LM) region, K458$_{Rc\text{-}o319}$ forms a salt-bridge with bACE2$_{R.cor}$ Glu35 (**Fig. 3G**). Distinctively, in this region, the Asn38-glycan is part of the ACE2-RBD interface, forming hydrogen bonds with N459$_{Rc\text{-}o319}$ (**Fig. 3G**). Also in this region, Lys353$_{Rc\text{-}o319}$ forms a hydrogen bond with the G461$_{Rc\text{-}o319}$ backbone (**Fig. 3G**). In the anchor-loop (AL) region, a hydrogen bond network is observed among ACE2 residues Tyr41, Asn330, Asp335, Arg357 and the RBD residue S465 (**Fig. 3H**). Further, the glycan attaching Asn38 is hydrogen bonded with bACE2$_{R.cor}$ residue Glu42 and RBD residue Y463$_{Rc\text{-}o319}$ (**Fig. 3H**). Finally, in the small-loop (SL) region, F423$_{Rc\text{-}o319}$ forms a sugar-π contact with the glycan attached to Asn38 (**Fig. 3I**).

These interactions, by comparison with those used by SARS-CoV-2 to engage ACE2 (**Fig. 3J-M**), show that Rc-o319 RBD engages its cognate bACE2$_{R.cor}$ receptor with unique characteristics.

Molecular determinates underlying Rc-o319 specificity for bACE2$_{R.cor}$

To understand the specificity of the Rc-o319 S-protein towards the bACE2$_{R.cor}$ receptor. We employed a systematic mutagenesis approach changing RBM regions to match that of SARS-CoV-2 (SL mutation = F423Y$_{Rc\text{-}o319}$; LM mutation = K458Q$_{Rc\text{-}o319}$; AL mutation = S465T$_{Rc\text{-}o319}$+A466N$_{Rc\text{-}o319}$+H470Y$_{Rc\text{-}o319}$). This approach has been previously used to elucidate how high-affinity hACE2 binding may be acquired by Type-2 sarbecovirus S-proteins (Wang et al., 2025). We found that changing AL and SL regions individually had very little effect in improving hACE2 binding (**Fig. 4D** and **E**). The SL change retained very strong bACE2$_{R.cor}$ utilization (**Fig. 4E, the third** and **fifth panels**), whereas the AL change substantially reduced bACE2$_{R.cor}$ utilization (**Fig. 4D, the third** and **fifth panels**).

Changing the LM region reduced bACE2$_{R.cor}$ utilization (**Fig. 4C, the first, third and fifth panels)** but failed to confer hACE2 mediated fusion activity (**Fig. 4C, the fourth panel**). Swapping of the Rc-o319 BL region to the LL sequence of SARS-CoV-2-RBD, appears to confer Rc-o319 with the ability to utilize hACE2 for cell fusion activity at the expense of substantially reduced fusion activity mediated by its cognate bACE2$_{R.cor}$ receptor (**Fig. 4B**). BLI assay results show that replacing BL with the LL sequence of SARS-CoV-2 greatly reduced bACE2$_{R.cor}$ receptor binding (**Fig. 4B, the first panel**). However, despite conferring cell fusion activity, binding of hACE2 is still too weak to be detected by the dimeric BL variant of Rc-o319-RBD-Fc protein **(Fig. 4B, the second panel** and **Figs. 7B)**. These findings are consistent with our previous observations that high-affinity hACE2 binding requires the RBD to establish optimal contacts across all the four RBM regions in the context of intact LL and SL. Optimal interactions across the 4 RBM regions act synergistically to confer high hACE2 affinity (Wang et al., 2025).

However, unexpectedly, when we tested the BL+LM+AL+SL variant, enhanced hACE utilization was observed in the cell-cell fusion assay but hACE2 binding was still too weak to be measured in the BLI assay (**Fig. 4F, the second** and **fourth panels**). The BL+LM+AL+SL variant Rc-o319-RBD-Fc protein also showed no bACE2$_{R.cor}$ binding in BLI assays, and consequently exhibited very little bACE2$_{R.cor}$ mediated fusion activity (**Fig. 4F, the first** and **third panels)**. Therefore, in the case of Rc-o319 S-protein, determinants outside of the BL, LM, AL, and SL regions likely hinder high-affinity hACE binding.

Structural comparison found that W430$_{\text{Rc-o319}}$ and S432$_{\text{Rc-o319}}$ within the large RBM-loop (amino acid (AA) 429-442$_{\text{Rc-o319}}$, corresponding to AA 455-468$_{\text{SARS2}}$) N-terminal to the BL are unique to Rc-o319 RBD (**Fig. 3F**, **Figs. 4G** and **6**). The corresponding residues are F456$_{\text{SARS2}}$ and K458$_{\text{SARS2}}$ in SARS-CoV-2 RBD; they respectively form interactions with the LL residues Y473$_{\text{SARS2}}$ and E471$_{\text{SARS2}}$ (**Fig. 3J** and **Figs. 6A** and **D**). These interactions likely stabilize the SARS-CoV-2 LL structure. We introduced these residues into the Rc-o319 BL+SL+LM+AL variant as W430F$_{\text{Rc-o319}}$ and S432K$_{\text{Rc-o319}}$ substitutions (collectively named as the "RBM-loop" mutation), the BLI binding results show that the dimeric

BL+SL+LM+AL+RBM-loop Rc-o319-RBD-Fc variant is able to bind hACE2 with a much increased affinity of 31.7 nM (**Fig. 4G**). We also attempted the swap of Rc-o319 RBM for the SARS-CoV-2 RBM (Rc-o319-RBD-RBM$_{SARS2}$), as expected, the variant Rc-o319-RBD-Fc with the swapped RBM also showed high-affinity binding to hACE2 with only slightly higher affinity (12.3 nM) than the BL+SL+LM+AL+RBM-loop variant (**Fig. 4H**). Consistently, both BL+SL+LM+AL+RBM-loop and RBM swapped Rc-o319-RBD-RBM$_{SARS2}$ show effective hACE2 mediated cell-fusion activities. Therefore, our mutagenesis results identify residues in the RBM-loop of Rc-o319 N-terminal to BL contain residues non-compatible with LL structure of the Type-1 RBD, thereby preventing the LL structure from mediating optimal ACE2 interaction (**Figs. 6C**).

Utilization of bACE2$_{R.cor}$ by different types of sarbecoviruses

Our structural and biochemical analyses show that the Rc-o319 S-protein has a highly restrictive specificity towards its cognate bACE2$_{R.cor}$ receptor, we further characterize the potential of bACE2$_{R.cor}$ to support diverse sarbecoviruses **(Fig. 4)**. A panel of sarbecovirus S-proteins was surface-expressed on effector cells and tested for cell-cell fusion activity against receptor cells expressing bACE2$_{R.cor}$ (**Fig. 4I**). The panel included Type-1 RBD S-proteins from SARS-CoV-1, LYRa11, SHC014, WIV1, RaTG13, BANAL-20-52, BANAL-20-236, and the SARS-CoV-2 ancestral strain; Type-2 RBD S-proteins from BtKY72, BM48-31, RfGB02, and RhGB07; and Type-3 RBD S-proteins from GX2013, HeB2013, YN2013, and RmYN02. The results show that bACE2$_{R.cor}$ can support receptor binding mediated cell fusion activities of several sarbecovirus S-proteins with Type-1 RBDs (**Fig. 4J** and **K**). However, stronger fusion activity was only observed for several S-proteins of viruses from the SARS-CoV-2 clade. SARS-CoV-1 S-protein was the only one demonstrated bACE2$_{R.cor}$ mediated cell-fusion activity within the SARS-CoV-1 clade (**Fig. 4I-K**). Among bACE2$_{R.cor}$ utilizing S-proteins, the BANAL20-236 S-trimer was found to bind bACE2$_{R.cor}$ in BLI assays, whereas S-trimers of BANAL-20-52, SARS-CoV-2 and SARS-CoV-1 showed no binding to bACE2$_{R.cor}$ **(Fig. 4K** and **Figs. 9B, C, E** and **F)**.

The Asn38-linked glycan in bACE2$_{R.cor}$ is involved in S-protein binding, a feature observed for the first time between an ACE2 and a sarbecovirus S-protein. To understand the effect of this glycan on S-protein binding, we removed the glycan by introducing a Thr40Ala change (designated as 'bACE2$_{R.cor}$-ΔGLC$_{38}$'). bACE2$_{R.cor}$-ΔGLC$_{38}$ appears to support enhanced cell fusion activities for S-proteins capable of utilizing bACE2$_{R.cor}$ **(Fig. 4J-K** and **Figs. 9A, C, E** and **H)**. BLI assay results show that the removal of the Asn38-glycan was able to enhance bACE2$_{R.cor}$ binding by monomeric RBDs and S-trimers of Rc-o319 and BANAL-20-236 in BLI assays (**Figs. 9A, E, J** and **K**), despite that the Asn38-glycan was found involved in the interface formed between bACE2$_{R.cor}$ and Rc-o319-RBD **(Fig. 3E, G** and **I)**. Further, although unable to utilize WT bACE2$_{R.cor}$, the Type-2 BtKY72 S-protein was found to utilize bACE2$_{R.cor}$-ΔGLC$_{38}$, albeit only showing very weak cell fusion activity. Consistently, BLI binding result shows that the BtKY72 S-trimer binds bACE2$_{R.cor}$-ΔGLC$_{38}$ with an estimated affinity of 11.8 nM (**Figs. 9H, the second panel)**. These data suggest that the Asn38-linked glycan, likely due to its bulky and branched structure, imposes steric hindrance on S-protein binding.

Discussion

In this study, our receptor binding and structural analyses show that Rc-o319 S-protein exhibits a clear preference for its cognate bACE2$_{R.cor}$ receptor with marked reduced utilization of *R. sinicus* and *R. affinis* ACE2 receptors. Rc-o319 S-protein showed no utilization of human and pangolin ACE2s. A closer relationship among Asian *Rhinolophus* bats (Chornelia & Hughes, 2022) probably allowed Rc-o319 S-protein to cross-bind *R. sinicus* and *R. affinis* ACE2s. Previously, it has been shown that weak binding of SARS-CoV-2 S-protein to mouse ACE2 (mACE2) was unable to facilitate effective mouse infection, and increased mACE2 binding was key to effective mouse infection (Shuai et al., 2021). Therefore, weak *R. sinicus* and *R. affinis* ACE2 binding may not allow effective infection of *R. sinicus* and *R. affinis* bats by the Rc-o319 virus.

Our structural analyses reveal that the Rc-o319 S-trimer adopts two distinct conformations: a locked-1 conformation with fatty-acid bound RBDs and a locked-2 conformation in which those fatty-acid binding pockets are unoccupied. Previous cryo-EM studies of bat sarbecovirus S-trimers have nearly always captured them in locked-2 conformations with and without fatty acid bound (Wang et al., 2025). Locked-1 conformation has only been reported for the bat sarbecovirus WIV1 S-trimer (Hills et al., 2024). Both locked-1 and locked-2 conformations have been observed for SARS-CoV-1 and SARS-CoV-2 S-trimers. The locked-1 conformation appears to be always identified with fatty acid bound, whereas the locked-2 conformation has been resolved with or without fatty acid bound. Interestingly, these two conformations appear to be more difficult to capture for SARS-CoV-1 (Zhang et al., 2023) and SARS-CoV-2 (Qu et al., 2022, Xiong et al., 2020, Zhou et al., 2020b) S-trimers and their capture often requires deliberate stabilization of the S-trimers. The predominance of locked conformations in bat sarbecovirus S-trimers, versus them being rare conformations in human-infecting sarbecoviruses, has been proposed to reflect likely differences in S-trimer stability (Wang et al., 2025). We have also proposed that tightly packed S-trimers in locked conformations facilitate viral egress (Qu et al., 2022). As the preferred conformation for bat sarbecovirus S-proteins, these locked conformations have also been postulated to represent adaptations for fecal-oral transmission and immune evasion in their natural hosts (Hills et al., 2024, Ou et al., 2023).

Due to residue-31 of bat ACE2 molecules often being a negative charged Asp or Glu, a positively charged LM region, such as $K458_{Rc\text{-}o319}$ (corresponding to $Q493_{SARS2}$), has been noted as an important determinant for specificity towards bACE2 (Li, 2008). Monomeric BANAL-20-236-RBD, with a K in the LM region, with the ability to bind a variety of bACE2 molecules (Ou et al., 2023), binds $bACE2_{Ra5538}$ with a moderate affinity of 104 nM (Wang et al., 2025). For comparison, it binds $bACE2_{R.cor}$ with a much reduced affinity of 937 nM **(Figs. 9K, the top panel)**. SARS-CoV-2-RBD is highly similar to BANAL-20-236, however, with a neutral Q in the LM region, SARS-CoV-2-RBD-Fc binding to $bACE2_{R.cor}$ could not be measured by the BLI assay. With a $Q493K_{SARS2}$ point mutation in LM, SARS-CoV-2-RBD-Fc binds $bACE2_{R.cor}$ in BLI assays (compare **Figs. 8H** and **L**). In addition, SARS-CoV-1-RBD-Fc with the $N482K_{SARS1}$ gained weak $bACE2_{R.cor}$

binding (**Figs. 8K**). These results are consistent with the LM change ($K458Q_{Rc\text{-}o319}$) in the Rc-o319 S-protein, which considerably reduced $bACE2_{R.cor}$ binding (**Fig. 4C**), suggesting that a positive-charged LM region contributes to high-affinity binding towards the $bACE2_{R.cor}$ receptor.

The Rc-o319-RBD:$bACE2_{R.cor}$ complex structure reveals that Rc-o319-RBD employs a featured beta-loop (BL) structure to bind the $bACE2_{R.cor}$ molecule using a previous unobserved novel interaction pattern. While this manuscript was in preparation, a preprint also reported a cryo-EM structure of Rc-o319 RBD:$bACE2_{R.cor}$ complex structure, confirming our observation (Kosugi et al., 2025). We show that replacing the Rc-o319 BL with the SARS-CoV-2 LL sequence has a greater impact on $bACE2_{R.cor}$ binding than various LM mutations (**Fig. 3B** vs **Fig. 3C** and see **Figs. 9D** for the $K458A_{Rc\text{-}o319}$ substitution), suggesting that the BL structure contributes greater to high-affinity binding towards the $bACE2_{R.cor}$ receptor in the Rc-o319 S-protein.

Our data show that the specialized BL loop co-adapts with the Rc-o319 RBM loop to confer high-affinity binding to its cognate $bACE2_{R.cor}$ receptor, but this co-adaptation renders the RBM-loop incompatible with the SARS-CoV-2 LL region **(Figs. 6C** and **F)**, preventing an introduced LL region from mediating high-affinity hACE2 binding in BLI **(**compare **Fig. 4F** and **G,** compare **Figs. 7C-D)**. Conversely, changing SARS-CoV-2 LL to the BL in Rc-o319-RBD completely abolishes hACE2 binding and $bACE2_{R.cor}$ binding (**Figs. 10A** and **E**), likely due to incompatibility between BL and RBM-loop. These observations further suggest that the Rc-o319 BL and RBM-loop are specialized structures adapted for $bACE2_{R.cor}$ binding, and their unique structural features and interactions engaged support classifying the Rc-o319-RBD as a novel Type-4 RBD. However, our data show the specialized BL and RBM-loop of the Rc-o319 RBM severely limit its capacity for high-affinity hACE2 binding, with extensive mutations and insertions in these regions likely required to achieve the binding affinity necessary for cross-species transmission.

Finally, our results show that, in contrast to the highly efficient utilization of bACE2$_{R.cor}$ by the Rc-o319 S-protein, bACE2$_{R.cor}$ supports only limited usage by selected sarbecovirus S-proteins with Type-1 RBDs. Notably, most of these S-proteins are from viruses that belong to the SARS-CoV-2 clade (Clade 1b), highlighting this clade's extraordinary ability to recognize a broad range of ACE2 orthologs. Albeit showing cell fusion activities, most bACE2$_{R.cor}$ utilizing S-proteins show weak binding of bACE2$_{R.cor}$ in BLI assays. Therefore, bACE2$_{R.\mathrm{cor}}$ appears to have evolved to permit efficient binding by the S-proteins of highly specific sarbecovirus species. Further, our data show that the Asn38-glycan of bACE2$_{R.cor}$ hinders sarbecovirus S-protein binding, likely further restricting its utilization as a receptor. Interestingly, the Asn38-linked glycan is also located within the binding interfaces of multiple ACE2-utilizing Merbecovirus S-proteins, and is therefore likely to restrict their binding (Chen et al., 2025b, Park et al., 2025).

In summary, the interaction between the Rc-o319 S-protein, featuring a specialized RBM, and bACE2$_{R.cor}$ reflects a highly specific co-adaptation between virus and host. To enable such adaptation, the RBM of Rc-o319 has diverged substantially from that of the SARS-CoV-2 lineage, to which it is most closely related, resulting in a highly restricted ACE2 specificity. Notably, the RBM is also a major target of immune pressure, as demonstrated by the ongoing evolution of SARS-CoV-2 (Chen et al., 2025a, He et al., 2022, Liu et al., 2024, Yan et al., 2024, Yu et al., 2023). Given that certain SARS-CoV-2 lineage viruses can utilize bACE2$_{R.cor}$, it remains unclear what evolutionary pressures, potentially including immune escape, have driven the Rc-o319 S-protein to specialize for its host receptor.

Materials and Methods

Reagents and Tools Table

Reagent/Resource	Reference or Source	Identifier or Catalog Number
Experimental Models		
Expi293F	Thermo Fisher Scientific	Cat# A14527
HEK293T	ATCC	Cat# CRL-3216
Recombinant DNA		
pQCXIP-GFP1-10	Addgene	Cat# 68715
pQCXIP-BSR-GFP11	Addgene	Cat# 68716
pCDNA3.1(+)	Thermo Fisher Scientific	Cat# V79020
pCDNA3.1-Rc-o319 RBD-Fc	This study	N/A
pCDNA3.1-SARS-CoV-2 RBD-Fc	(Wang et al., 2025)	N/A
pCDNA3.1-Rc-o319 spike	This study	N/A
pCDNA3.1-hACE2-6his	(Wang et al., 2025)	N/A
pCDNA3.1-*Rhinolophus cornutus* bACE2-6his	This study	N/A
pCDNA3.1-*Rhinolophus ferrumequinum* bACE2-6his	(Guo et al., 2020)	N/A
pCDNA3.1-*Myotis lucifugus* bACE2-6his	(Tan et al., 2023)	N/A
pCDNA3.1-pangolin ACE2-6his	(Guo et al., 2020)	N/A
pCDNA3.1-*Ra9479* bACE2-6his	(Guo et al., 2020)	N/A
pCDNA3.1-*Ra5538* bACE2-6his	(Guo et al., 2020)	N/A
pCDNA3.1-*Rs*-WJ2 bACE2-6his	(Guo et al., 2020)	N/A
pCDNA3.1-*Rs1434* bACE2-6his	(Guo et al., 2020)	N/A
pCDNA3.1-*Rs1438* bACE2-6his	(Guo et al., 2020)	N/A
pCDNA3.1-*Rs1446* bACE2-6his	(Guo et al., 2020)	N/A
pCDNA3.1-*Rs3357* bACE2-6his	(Guo et al., 2020)	N/A
pCDNA3.1-*Rs3359* bACE2-6his	(Guo et al., 2020)	N/A
pCDNA3.1-*Rs3366* bACE2-6his	(Guo et al., 2020)	N/A
pCDNA3.1-*Rs5720* bACE2-6his	(Guo et al., 2020)	N/A
Antibodies		
Binds to FLAG® Tag epitope) Antibody	Sino Biological	Cat# 109143-MM13
SARS-CoV-2 (2019-nCoV) Spike S2 Antibody	Sino Biological	Cat# 40590-T62
Goat anti-rabbit IgG (H+L)-HRP	Jackson ImmunoResearch	Cat# 111-035-003
Oligonucleotides and		

other sequence-based reagents		
Oligonucleotides		
Rc-o319-RBD-Fc-F: TGCTGGTCGCTTCCGTGctagctAGAGTGCAGCCCCAGGACACCG	This study	N/A
Rc-o319-RBD-Fc-R: AGAACAAGTGCGTGAACTTCCCCCTGGTGCCCAGAGGCTCCG	This study	N/A
Rc-o319-spike-6P-F779P-F: CCCTCTAAGCGGAGCCCCATCGAGGACCTGCTGTTTAATAAGGT	This study	N/A
Rc-o319-spike-6P-F779P-R: CTTATTAAACAGCAGGTCCTCGATGGGGCTCCGCTTAGAGGGCTT	This study	N/A
Rc-o319-spike-6P-A854PA855P-F: ACCTTCGGCGCCGGCCCCCCCCTGCAGATTCCCTTCGCCATGCAGATG	This study	N/A
Rc-o319-spike-6P-A854PA855P-R: TCTGCATGGCGAAGGGAATCTGCAGGGGGGGGCCGGCGCCGAAGGTC	This study	N/A
Rc-o319-spike-6P-Rc-A904P-F: TCCCTGACCTCCACCCCCAGCGCCCTGGGCAAGCTGC	This study	N/A
Rc-o319-spike-6P-Rc-A904P-R: AGCTTGCCCAGGGCGCTGGGGGTGGAGGTCAGGGACTC	This study	N/A
Rc-o319-spike-6P-Rc-K948PV949P-F: CATCAGCAGGCTGGACCCGCCGGAGGCCGAGGTGCAGATCGACC	This study	N/A
Rc-o319-spike-6P-Rc-K948PV949P- R: TCGATCTGCACCTCGGCCTCCGGCGGGTCCAGCCTGCTGATGATG	This study	N/A
Rc-o319-BL mutation-F: AGCACCGAGATTTACCAGGCCGGCAGCACCCCATGCAACGGCGTGGAGGGCTTCAACTGCTACTTCCCACTGAAGAATTACGGCTTTTATAGCTC	This study	N/A
Rc-o319-BL mutation-R: TGGGAAGTAGCAGTTGAAGCCCTCCACGCCGTTGCATGGGGTGCTGCCGGCCTGGTAAATCTCGGTGCTAATGTCGCGCTCAAAAGGCCTCAGCT	This study	N/A
Rc-o319-LM mutation-F: AGTTTAAGAGCAGCCTGCAGAATTATGGCTTTTACTCTAGCG	This study	N/A
Rc-o319-LM mutation-R: AGCCATAATTCTGCAGGCTGCTCTTAAACTGGGTG	This study	N/A
Rc-o319-AL-S465T-A466N-H470Y mutation-F: TTATGGCTTTTACTCTACCAACGGCGATAGCTACCAGCCTTACAGAGTG	This study	N/A
Rc-o319-AL-S465T-A466N-H470Y mutation-R: ACCACTCTGTAAGGCTGGTAGCTATCGCCGTTGGTAGAGTAAAAGCCAT	This study	N/A
Rc-o319-SL-F423Y mutation-F: CTACCAGCGGCAATTATAATTATTACTA	This study	N/A

CAGA		
Rc-o319-SL-F423Y mutation-R: TCTGTAGTAATAATTATAATTGCCGCTGGTA	This study	N/A
Rc-o319-RBM-loop$_{SARS2}$ mutation-F: CTATAGAATCTTCCGCAAGGAGAAGCTGAGGCCTTTTGAG	This study	N/A
Rc-o319-RBM-loop$_{SARS2}$ mutation-R: GGCCTCAGCTTCTCCTTGCGGAAGATTCTATAGTAGTAGTTG	This study	N/A
Rc-o319-RBM$_{SARS2}$ mutation-F: TGCGTGCTGGCCTGGAACTCTAACAACCTCGACTC	This study	N/A
Rc-o319-RBM$_{SARS2}$ mutation-R: AAGCTCAGCACCACCACCCGGTATGGCTGGTAGCCCACGC	This study	N/A
Rc-o319-K454Y mutation-F: GGTGGGCACCCAGTTTTATAGCAGCCTGAAGAATTA	This study	N/A
Rc-o319-K454Y mutation-R: CATAATTCTTCAGGCTGCTATAAAACTGGGTGCCCAC	This study	N/A
Rc-o319-K458A mutation-F: CAGTTCAAGTCCAGCCTGGCGAATTACGGCTTTTATAGCT	This study	N/A
Rc-o319-K458A mutation-R: GTAATTCTTCAGGCTGGACGCGAACTGTGTGCCCACCTGGT	This study	N/A
SARS2-BL$_{Rc\text{-}o319}$ mutation-F: GCCCACTATGATTACCAGGTGGGCACACAGTTCAAGTCCAGCCTCCAGTCTTACGGCTTCCAGCCTACAA	This study	N/A
SARS2-BL$_{Rc\text{-}o319}$ mutation-R: GCTGGACTTGAACTGTGTGCCCACCTGGTAATCATAGTGGGCAATGTCCCGCTCGAAAGGCTTCAGGTTAGACTT	This study	N/A
SARS2-Q493K-F: TACTTTCCCCTCAAGAGCTACGGCTTCCAACCCACCAACGGCGTG	This study	N/A
SARS2-Q493K-R: TGGTGGGTTGGAAGCCGTAGCTCTTGAGGGGAAAGTAGCAGTTAAAGCCC	This study	N/A
SARS2-RBM-loop$_{Rc\text{-}o319}$-F CAGGCTGCGTGATCGCCTGGAATAGCAGAAACCAGGACGC	This study	N/A
SARS2-RBM-loop$_{Rc\text{-}o319}$-R CAAAAGACAGCACCACCACCCGGTAGGGCTGGTGAGAGTCGC	This study	N/A
Rhinolophus cornutus bACE2-6his-F: CGTGGCCGAGACCGGGACAAGCACCACCGAGGACGAGGCCAAGAAGTTCCTGAATGAC	This study	N/A
Rhinolophus cornutus bACE2-6his-R: GGAGCCTCTGGGCACCAGGGGGGTCACGGGAGGCTGGTAGGGG	This study	N/A
Rhinolophus cornutus bACE2-Fc-F: GATGCTGGTCGCTTCCGTGCTAGCTAGCACCACCGAGGACGAGGCCAAG	This study	N/A
Rhinolophus cornutus bACE2-Fc-R: TGGCCCTCGTCCTCGGTGGTGCTAGCTA	This study	N/A

GCACGGAAGCGACCAGCATCCC		
Rhinolophus cornutus bACE2-Fc-T40A-F: GAGGCCGAGAACCTGGCCTACCAGTCATCCCTGGCCTGCTGGG	This study	N/A
Rhinolophus cornutus bACE2-Fc-T40A-R: CAGCTGGCCAGGGATGACTGGTAGGCCAGGTTCTCGGCCTCGAATTTAA	This study	N/A
Chemicals, Enzymes and other reagents		
Protein A agarose	Genscript	Cat# L00433-55
Expi293F culture medium	ThermoFisher Scientific	Cat# A1435101
Polyethylenimine	Polysciences	Cat# 24765-1
PBS, pH 7.0	Gibco	Cat# C10010500CP
2 × Taq Master Mix (Dye Plus)	Vazyme	Cat# P112-01
ClonExpress Ultra One Step Cloning Kit V3	Vazyme	Cat# C117-01
Software		
GraphPad Prism v8.0	GraphPad	https://www.graphpad.com/
Data Analysis HT v12.0.2.59 software	Sartorius	N/A
CryoSPARC	(Punjani et al., 2017)	https://cryosparc.com/
UCSF Chimera v1.15	(Pettersen et al., 2004)	http://plato.cgl.ucsf.edu/chimera/
PHENIX v1.19.1	(Afonine et al., 2018)	https://www.phenix-online.org/
Coot v0.9.8.1	(Emsley et al., 2010)	http://www2.mrc-lmb.cam.ac.uk/personal/pemsley/coot/
Other		
HiTrap TALON crude column	Cytiva	Cat# 28953766
HiTrap Protein A HP column	Cytiva	Cat# 17040301
Protein A biosensors	Sartorius	Cat# 18-5010
R1.2/1.3 300 mesh Cu holey carbon grids	Quantifoil	Cat# Q350CR1.3

Methods and protocols

Protein constructs

S gene of Rc-o319 (Taxonomy ID: 694009) was codon-optimized and synthesized by Sangon Biotech (Shanghai, China). The transmembrane domain and C-terminal end of Rc-o319 (AA 1176-1235) were removed before the C-terminus of the

coding sequence was fused to a T4 trimerization foldon, an HRV3C cleavage site, an Octo-His tag, and a double strep-tag to allow secretory expression and purification.

Rhinolophus cornutus (*R.cor*, Genebank: BCG67443.1), human (hACE2, Genebank: BAB40370.1), *Rhinolophus ferrumequinum* (*R.ferr*, Genbank: BAH02663.1) and greater mouse-eared bat *Myotis lucifugus* (*M.luci*, Genbank: XP_023609438.1) ACE genes were synthesized. Pangolin (Pangolin, Genbank: XP_017505752.1), *Rhinolophus affinis* 9479 (*Ra9479*, Genbank: QMQ39227), *Rhinolophus affinis* 787 (*Ra5538*, Genbank: QMQ39222), *Rhinolophus sinicus* WJ2 (*Rs*-WJ2, Genbank: QMQ39202.1), *Rhinolophus sinicus* 1434 (*Rs*1434, Genbank: QMQ39216.1), *Rhinolophus sinicus* 1438 (*Rs*1438, Genbank: QMQ39203.1), *Rhinolophus sinicus* 1446 (*Rs*1446 Genbank: MT394194.1), *Rhinolophus sinicus* 3357 (*Rs*3357 Genbank: AGZ48803.1), *Rhinolophus sinicus* 3359 (*Rs*3359 Genbank: QMQ39211.1), *Rhinolophus sinicus* 3366 (*Rs*3366, Genbank: QMQ39215.1) and *Rhinolophus sinicus* 5720 (*Rs*5720, Genbank: MT394182.1) ACE2 gene sequences were from a previous study (Guo et al., 2020). The peptidase domain and the C-terminal collectrin-like domain of ACE2, bearing a carboxy-terminal Hexa-His tag, was generated for hACE2. Due to the presence of the C-terminal collectrin-like domain, these his-tagged ACE2 (AA 1-731) proteins form dimers. Additionally, the same length of ACE2s were fused to the Fc domain of human IgG with one thrombin site and a GGGG linker in between, resulting in Fc-tagged ACE2.

Rc-o319 RBD and variants (AA 293-506), SARS-CoV-2 RBD (AA 319-541), were fused with human IgG Fc domains to generate dimeric RBD-Fc proteins.

Protein expression and purification

Proteins were expressed by transient transfection in Expi293F cells, 1 mg of DNA was transfected into 1 L of cells using Linear Polyethylenimine (PEI) transfection reagent. After transfection, cells were cultured at 33 °C for 4 days for S-proteins, 5 days for RBD and ACE2 proteins. For his-tagged S-proteins and RBD proteins, the supernatants were harvested by centrifugation and 25 mM phosphate pH 8.0, 3 mM imidazole, 300 mM NaCl, and 0.5 mM PMSF were supplemented. Supernatant was recirculated onto a 5-ml Talon Cobalt column for about 3 times

and the column was washed by 100 ml buffer A (25 mM phosphate pH 8.0, 5 mM imidazole, and 300 mM NaCl). Proteins were eluted using a linear gradient with increasing concentration of Buffer B (25 mM phosphate pH 8.0, 500 mM imidazole, and 300 mM NaCl). Eluted protein samples were quality checked by SDS-PAGE, concentrated and buffer-exchanged into PBS using a 100 kDa (for S-proteins) or 10 kDa (for RBD proteins) MWCO Amicon Ultra filtration device (Merck Millipore). The concentrated proteins were frozen in liquid nitrogen and stored at -80 °C.

For RBD-Fc and ACE2-Fc proteins, 5 days post-transfection, each culture supernatant was cleared by filtering through a 0.45 μm filter membrane before being loaded onto a 5 mL HiTrap Protein A column (Cytiva). The column was washed by PBS (10 mM Na_2HPO_4 and 1.8 mM KH_2PO_4 pH 7.4, 137 mM NaCl, and 2.7mM KCl). Proteins were eluted using a linear gradient with increasing concentration of a citrate buffer (0.1 M citric acid, pH 3.0). Eluted protein fractions were immediately neutralized with equal volumes of 1.0 M Tris-HCl pH 8.0 buffer. RBD-Fc and ACE2-Fc proteins were concentrated, buffer-exchanged into PBS before being frozen and stored at -80 °C.

Biolayer Interferometry (BLI) binding analysis

Binding of Rc-o319 S-proteins or RBDs to ACE2-Fc proteins was assessed using biolayer interferometry (BLI) on an Octet RED 96 instrument (FortéBio, USA). All steps were performed at 25 °C with an orbital shaking speed of 1000 rpm. All reagents were formulated in PBS-TB buffer (PBS with 0.02% v/v Tween-20 and 0.1% w/v BSA). Before the experiments, all protein A biosensors were pre-equilibrated in the PBS-TB buffer for 10 min. ACE2-Fc proteins (11 μg/ml) were immobilized onto Protein A biosensors (FortéBio, USA) to a response value of ~1.2 nm. After a 60 s baseline step in PBS-TB, the biosensors immobilized with ACE2-Fc proteins were submerged in the analyte (S-proteins or RBDs) solutions for 300 s to measure association, before being submerged in PBS-TB for 600 s to measure dissociation. Data were reference subtracted and analyzed in the FortéBio Data Analysis Software (FortéBio) by fitting to 1:1 or 2:1 binding models to determine k_{on}, k_{off}, and K_D values as previously described (Carnell et al., 2021). Raw data and fits were plotted using GraphPad Prism 8 (GraphPad Software).

Binding of dimeric his-tagged hACE2, pangolin ACE2, and bACE2s to Rc-o319 RBD-Fc protein was assessed using the BLI assay. The RBD-Fc proteins (11 μg/ml) were loaded onto Protein A biosensors (FortéBio, USA) to a level of ~1.2 nm. After a 60 s baseline step in PBS-TB buffer, the biosensors immobilized with RBD-Fc proteins were submerged in the ACE2 protein solutions for 300 s to measure association, before being submerged in PBS-TB for 600 s to measure dissociation. Data were reference subtracted and analyzed in the FortéBio Data Analysis Software.

Cryo-EM grid preparation and data acquisition

Cryo-EM grids were prepared with Rc-o319 S-trimer samples at concentration of 1.65 mg/ml. All grids were prepared by applying 3.0 μl of S-trimer solutions directly to glow discharged (15 mA, 30 s) holey carbon grids (Quantifoil Cu mesh 300 R1.2/R1.3) before blotting. Cryo-EM grids were blotted for 2.5 s with a blot force of 4, before being plunge-frozen into liquid ethane using a Vitrobot Mark IV (ThermoFisher) at 4 °C and 100% humidity.

For Rc-o319 S-proteins, micrographs were collected using the EPU software (Thermo Fisher) on a Titan Krios G3i electron microscope (Thermo Fisher) operated at 300 keV. Micrographs were recorded at a nominal magnification of 130,000× on a Falcon 4 direct electron detector coupled to a Selectris-X energy filter set with a slit width of 10 eV and with a defocus range between -0.8 to -2.0 μm. Each movie was collected with a dose rate of 25 e^-/pixel/second, and exposed for 2.28 seconds, resulting in a total dose of 50 $e^-/Å^2$ with a calibrated pixel size of 0.93 Å.

For complex formation, wild-type dimeric Rc-o319 RBD was mixed with dimeric Fc-tagged $bACE2_{R.cor}$ at a 1.2:1 molar ratio, followed by incubation at 4 °C in the presence of 0.01% glutaraldehyde for 20 min. The glutaraldehyde was quenched by adding Tris-HCl to a final concentration of 50 mM. Gel filtration was performed to remove excess RBD on a Superose 6 10/300 GL column (Cytiva) equilibrated in PBS buffer. Complex formation was confirmed by SDS-PAGE, and the Rc-o319-RBD:$bACE2_{R.cor}$ complex peak was collected and concentrated to prepare cryo-EM grids. 3 μL of 6.8mg/mL the RBD-ACE2 complex was mixed with 8 mM 3-[(3-Cholamidopropyl)dimethylammonio]-2-hydroxy-1-

propanesulfonate (CHAPSO) before being applied onto glow discharged (15 mA, 30 s) Ni-Au-300 mesh R1.2/1.3 grids. Grids were blotted for 2.5 s with a blot force of 5 before being plunge frozen into liquid ethane using a Vitrobot Mark IV (Thermo Fisher Scientific) at 4 °C and 100% humidity. Micrographs were collected on a Titan Krios electron microscope (Thermo Fisher) operated at 300 keV using the EPU software (Thermo Fisher). Micrographs were recorded at a nominal magnification of 130,000× on a K3 direct electron detector (Gatan) coupled to a Gatan BioQuantum energy filter set with a slit width of 20 eV (Thermo Fisher) and with a defocus range between -0.8 to -2.0 μm. Each movie was collected with a dose rate of 18.7 e^-/pixel/second, exposed for 1.78 seconds, resulting in a total dose of 50 $e^-/Å^2$ with a calibrated pixel size of 0.65 Å.

Image processing

For dataset processed by the CryoSPARC package (Punjani et al., 2017), particles were picked before 2D classification was performed. Well featured particles from the 2D classification were subjected to *ab initio* 3D classification. Homogeneous Refinement and Local Refinement were applied to the set of particles with good features identified by the *ab initio* 3D classification.

For the Rc-o319-RBD:bACE2$_{R.cor}$ complex dataset, data processing was performed mainly using cryoSPARC (Punjani et al., 2017). After patch-motion correction and CTF estimation, micrographs with CTF fit resolution above 6Å were picked by the curate exposures job. Particles were then picked using a blob picker to generate templates for the subsequent template picker. Picked particles were extracted at 3x binning and subjected to 2D classification, *ab initio* reconstruction, and heterogeneous refinement. Particles belongs to classes with high-resolution details were selected for a final round of Topaz picker by the Topaz cross validation job. Picked particles were extracted at 3x binning and subjected to 2D classification, *ab initio* reconstruction, and heterogeneous refinement again. Highly similar classes in heterogeneous refinement showing high-resolution details were combined and re-extracted at 1.5x binning and subjected to non-uniform refinement with optimization of per-group CTF parameter analysis. The CTF-refined particles and volumes were subjected to reference-based motion correction and an extra round of non-uniform refinement to get the final dimeric structure.

Due to conformational dynamics in the dimeric RBD-ACE2 complex structure, several local regions were resolved to lower resolution. Local refinement was applied to improve the local resolution at the RBD-ACE2 binding interface. Particles were symmetry expanded, the dynamic parts were masked, before the particles were subtracted through masking. The subtracted particles were imported to perform NU-Refine and local refinement jobs.

Model building and structure refinement

A previous determined SARS-CoV-2 S-trimer structure (PDB ID: 6ZP2) (Xiong et al., 2020) was used as the starting models for the Rc-o319 S-trimer structures. Model building and adjustment were performed manually in Coot 0.9 (Emsley et al., 2010). Steric clash and sidechain rotamer conformations were improved using the Namdinator web server (Kidmose et al., 2019). Final structures after additional manual adjustments were refined and validated in PHENIX-1.18.261 (Afonine et al., 2018). The SARS-CoV-2-RBD:hACE2-B^0AT1 complex structure (PDB ID: 6M17, EMD-30039) (Buchrieser et al., 2020, Yan et al., 2020) was used as the starting model for the Rc-o319 RBD:bACE2$_{R.cor}$ complex structure. The starting model was fitted in the cryo-EM density in Chimera before manual adjustments were carried out in Coot. The model was refined by multiple rounds of refinement in Namdinator and PHENIX. Data collection and refinement statistics for all the reported structures are provided in Table S1.

GFP-split fusion assay

The split-GFP system based cell-cell fusion assay mediated by the interaction between the S-protein and the ACE2 receptor was previously described (Ma et al., 2023). Briefly, HEK293T cells transfected with full length S-proteins and pQCXIP-GFP1-10 were prepared as effector cells, while HEK293T cells transfected with bat ACE2 (*R.cor*, *Rs*-WJ2, *Rs*1446, *Rs*1434, *Rs*1438, *Rs*3357, *Rs*3366, *Rs*3359, *Rs*5720, *Ra*9479, *Ra*5538, *R.ferr*, and *M.luci*) or pangolin ACE2 or human ACE2 (hACE2) and pQCXIP-BSR-GFP11 served as receptor cells. 24 h after transfection, effector and receptor cells were washed and resuspended in DMEM containing 10% FBS without trypsin treatment, mixed at a 1:1 ratio, and plated at ~2×10^5 cells per well in a 96-well plate. Fluorescence images were recorded at the indicated time points using a Nikon TS2-S-SM fluorescence

microscope. The GFP area was quantified with ImageJ. S-protein expression was analyzed via flow cytometry using a SARS-CoV-2 S2 antibody (1:2500 dilution, Sino Biological, 40590-T62) and Western blot using an anti-FLAG antibody (1:1000 dilution, Sino Biological, 109143-MM13). The GFP area was normalized to the mean fluorescence intensity of surface S-proteins.

Data availability

Cryo-EM density maps and coordinates generated in this study have been deposited in the Electron Microscopy Data Bank (EMDB; www.ebi.ac.uk/emdb/) and the Protein Data Bank (PDB; www.rcsb.org/ with the following accession numbers: Rc-o319 locked-1 S-trimer: EMD-65717 and PDB:9W75; Rc-o319 locked-2 S-trimer: EMD-65718 and PDB: 9W76; Dimeric Rc-o319-RBD:bACE2$_{R.cor}$ complex: EMD-65719 and PDB: 9W77, monomeric Rc-o319-RBD:bACE2$_{R.cor}$ complex: EMD65720 and PDB: 9W78. All data needed to evaluate the conclusions in the paper are present in the paper and/or the Supplementary Materials.

Acknowledgments

We thank the staff of the GIBH-CAS Cryo-EM Facility for their help with cryo-EM sample preparation and data collection. We thank the staff of the Guangzhou Laboratory Cryo-EM Facility for their help with cryo-EM sample data collection. This work was supported by the National Key R&D Program of China (2021YFA1300903 to X.X.); the National Natural Science Foundation of China (82341085 to X.X.); the Emergency Key Program of Guangzhou Laboratory (EKPG21–06 to X.X.); the R&D Program of Guangzhou National Laboratory (SRPG22–002 to X.X. and SRPG22-003 to J.H); the Guangdong Basic and Applied Basic Research Foundation (2021A1515011289 to X.X.); the Science and Technology Planning Project of Guangdong Province, China (2023B1212060050 to X.X., 2023B1212120009 to X.X.); the Basic Research Project of Guangzhou Institutes of Biomedicine and Health, Chinese Academy of Sciences (GIBHBRP24-02 to X.X.); the Natural Science Fund of Guangdong Province (2022A1515110211 to J.W.); the Young Doctoral Starting Sail Project of the Guangzhou Municipal Science and Technology Bureau (2024A04J4197 to J.W., 2024A04J4357 to Y.M.); and the Grants from State Key Laboratory of Respiratory Diseases (SKLRD-Z-202515 to Y.M.). X.X. acknowledges Start-up grants from the Chinese Academy of Sciences.

Author contributions

J.W., Z.L., and Y.M. conceived the study under the direction of X.C. and X.X. J.W. and Z.L. performed the clone design, protein purification and EM-structure

determination study; Y.M. performed the cell-cell fusion and FCAS assays; Z. L. and H.Y. performed BLI assays; J.W., B.L., C.N. and X.X. analysied the BLI results; J.W., Z.L., M.L., H.F. and M.Z. helped collect cryo-EM data under the supervision of J.H.and X.X.; Z.L., Zimu Li and J.W. processed cryo-EM data under the supervision of X.X.; J.W. Z.L. and X.X. analyzed cryo-EM structures; J.W., Z.L. and Y.M. prepared the figures under the supervision of X.X.; J.W., Z.L., Y.M. and X.X. wrote the paper with input from all authors; J.C. and J.H. reviewed and edited the manuscript; X.C. and X.X. supervised the research.

Conflict of interest

The authors declare no competing interests.

References

Afonine PV, Poon BK, Read RJ, Sobolev OV, Terwilliger TC, Urzhumtsev A, Adams PD (2018) Real-space refinement in PHENIX for cryo-EM and crystallography. *Acta Crystallogr D Struct Biol* 74: 531-544

Alkhovsky S, Lenshin S, Romashin A, Vishnevskaya T, Vyshemirsky O, Bulycheva Y, Lvov D, Gitelman A (2022) SARS-like Coronaviruses in Horseshoe Bats (Rhinolophus spp.) in Russia, 2020. *Viruses* 14: 113

Bosch BJ, van der Zee R, de Haan CA, Rottier PJ (2003) The coronavirus spike protein is a class I virus fusion protein: structural and functional characterization of the fusion core complex. *J Virol* 77: 8801-11

Buchrieser J, Dufloo J, Hubert M, Monel B, Planas D, Rajah MM, Planchais C, Porrot F, Guivel-Benhassine F, Van der Werf S, Casartelli N, Mouquet H, Bruel T, Schwartz O (2020) Syncytia formation by SARS-CoV-2-infected cells. *EMBO J* 39: e106267

Cai Y, Zhang J, Xiao T, Peng H, Sterling SM, Walsh RM, Jr., Rawson S, Rits-Volloch S, Chen B (2020) Distinct conformational states of SARS-CoV-2 spike protein. *Science* 369: 1586-1592

Carnell GW, Ciazynska KA, Wells DA, Xiong X, Aguinam ET, McLaughlin SH, Mallery D, Ebrahimi S, Ceron-Gutierrez L, Asbach B, Einhauser S, Wagner R, James LC, Doffinger R, Heeney JL, Briggs JAG (2021) SARS-CoV-2 Spike Protein Stabilized in the Closed State Induces Potent Neutralizing Responses. *J Virol* 95: e0020321

Chen B, Farzan M, Choe H (2025a) SARS-CoV-2 spike protein: structure, viral entry and variants. *Nat Rev Microbiol* 23: 455-468

Chen J, Zhang W, Li Y, Liu C, Dong T, Chen H, Wu C, Su J, Li B, Zhang W, Hu B, Jia J, Ma CB, Zhu Y, He X, Li A, Pan K, Lin H, Guo Z, Li C et al. (2025b) Bat-infecting merbecovirus HKU5-CoV lineage 2 can use human ACE2 as a cell entry receptor. *Cell* 188: 1729-1742 e16

Chornelia A, Hughes AC (2022) The evolutionary history and ancestral biogeographic range estimation of old-world Rhinolophidae and Hipposideridae (Chiroptera). *BMC Ecol Evol* 22: 112

Crook JM, Murphy I, Carter DP, Pullan ST, Carroll M, Vipond R, Cunningham AA, Bell D (2021) Metagenomic identification of a new sarbecovirus from horseshoe bats in Europe. *Scientific Reports* 11: 14723

Dadonaite B, Brown J, McMahon TE, Farrell AG, Figgins MD, Asarnow D, Stewart C, Lee J, Logue J, Bedford T, Murrell B, Chu HY, Veesler D, Bloom JD (2024) Spike deep mutational scanning helps predict success of SARS-CoV-2 clades. *Nature* 631: 617-626

Delaune D, Hul V, Karlsson EA, Hassanin A, Ou TP, Baidaliuk A, Gambaro F, Prot M, Tu VT, Chea S, Keatts L, Mazet J, Johnson CK, Buchy P, Dussart P, Goldstein T, Simon-Loriere E, Duong V (2021) A novel SARS-CoV-2 related coronavirus in bats from Cambodia. *Nat Commun* 12: 6563

Drexler JF, Gloza-Rausch F, Glende J, Corman VM, Muth D, Goettsche M, Seebens A, Niedrig M, Pfefferle S, Yordanov S, Zhelyazkov L, Hermanns U, Vallo P, Lukashev A, Muller MA, Deng H, Herrler G, Drosten C (2010) Genomic characterization of severe acute respiratory syndrome-related coronavirus in European bats and classification of coronaviruses based on partial RNA-dependent RNA polymerase gene sequences. *J Virol* 84: 11336-49

Drosten C, Gunther S, Preiser W, van der Werf S, Brodt HR, Becker S, Rabenau H, Panning M, Kolesnikova L, Fouchier RA, Berger A, Burguiere AM, Cinatl J, Eickmann M, Escriou N, Grywna K, Kramme S, Manuguerra JC, Muller S, Rickerts V et al. (2003) Identification of a novel coronavirus in patients with severe acute respiratory syndrome. *N Engl J Med* 348: 1967-76

Emsley P, Lohkamp B, Scott WG, Cowtan K (2010) Features and development of Coot. *Acta Crystallogr D Biol Crystallogr* 66: 486-501

Fouchier RA, Kuiken T, Schutten M, van Amerongen G, van Doornum GJ, van den Hoogen BG, Peiris M, Lim W, Stohr K, Osterhaus AD (2003) Aetiology: Koch's postulates fulfilled for SARS virus. *Nature* 423: 240

Freeman SL, Oliveira ASF, Gallio AE, Rosa A, Simitakou MK, Arthur CJ, Mulholland AJ, Cherepanov P, Raven EL (2023) Heme binding to the SARS-CoV-2 spike glycoprotein. *J Biol Chem* 299: 105014

Ge XY, Li JL, Yang XL, Chmura AA, Zhu G, Epstein JH, Mazet JK, Hu B, Zhang W, Peng C, Zhang YJ, Luo CM, Tan B, Wang N, Zhu Y, Crameri G, Zhang SY, Wang LF, Daszak P, Shi ZL (2013) Isolation and characterization of a bat SARS-like coronavirus that uses the ACE2 receptor. *Nature* 503: 535-8

Gui M, Song W, Zhou H, Xu J, Chen S, Xiang Y, Wang X (2017) Cryo-electron microscopy structures of the SARS-CoV spike glycoprotein reveal a prerequisite conformational state for receptor binding. *Cell Res* 27: 119-129

Guo H, Hu BJ, Yang XL, Zeng LP, Li B, Ouyang SY, Shi ZL (2020) Evolutionary Arms Race between Virus and Host Drives Genetic Diversity in Bat Severe Acute Respiratory Syndrome-Related Coronavirus Spike Genes. *J Virol* 94

Guo H, Li A, Dong TY, Si HR, Hu B, Li B, Zhu Y, Shi ZL, Letko M (2023) Isolation of ACE2-dependent and -independent sarbecoviruses from Chinese horseshoe bats. *J Virol* 97: e0039523

Han P, Su C, Zhang Y, Bai C, Zheng A, Qiao C, Wang Q, Niu S, Chen Q, Zhang Y, Li W, Liao H, Li J, Zhang Z, Cho H, Yang M, Rong X, Hu Y, Huang N, Yan J et al. (2021) Molecular insights into receptor binding of recent emerging SARS-CoV-2 variants. *Nat Commun* 12: 6103

Harrison SC (2008) Viral membrane fusion. *Nat Struct Mol Biol* 15: 690-8

Harvey WT, Carabelli AM, Jackson B, Gupta RK, Thomson EC, Harrison EM, Ludden C, Reeve R, Rambaut A, Consortium C-GU, Peacock SJ, Robertson DL (2021) SARS-CoV-2 variants, spike mutations and immune escape. *Nat Rev Microbiol* 19: 409-424

He P, Liu B, Gao X, Yan Q, Pei R, Sun J, Chen Q, Hou R, Li Z, Zhang Y, Zhao J, Sun H, Feng B, Wang Q, Yi H, Hu P, Li P, Zhang Y, Chen Z, Niu X et al. (2022) SARS-CoV-2 Delta and Omicron variants evade population antibody response by mutations in a single spike epitope. *Nat Microbiol* 7: 1635-1649

Hills FR, Eruera AR, Hodgkinson-Bean J, Jorge F, Easingwood R, Brown SHJ, Bouwer JC, Li YP, Burga LN, Bostina M (2024) Variation in structural motifs within SARS-related coronavirus spike proteins. *PLoS Pathog* 20: e1012158

Hu B, Ge X, Wang LF, Shi Z (2015) Bat origin of human coronaviruses. *Virol J* 12: 221

Hu Y, Liu K, Han P, Xu Z, Zheng A, Pan X, Jia Y, Su C, Tang L, Wu L, Bai B, Zhao X, Tian D, Chen Z, Qi J, Wang Q, Gao GF (2022) Host range and structural analysis of bat-origin RshSTT182/200 coronavirus binding to human ACE2 and its animal orthologs. *EMBO J*: e111737

Ke Z, Oton J, Qu K, Cortese M, Zila V, McKeane L, Nakane T, Zivanov J, Neufeldt CJ, Cerikan B, Lu JM, Peukes J, Xiong X, Krausslich HG, Scheres SHW, Bartenschlager R, Briggs JAG (2020) Structures and distributions of SARS-CoV-2 spike proteins on intact virions. *Nature* 588: 498-502

Kidmose RT, Juhl J, Nissen P, Boesen T, Karlsen JL, Pedersen BP (2019) Namdinator - automatic molecular dynamics flexible fitting of structural models into cryo-EM and crystallography experimental maps. *IUCrJ* 6: 526-531

Kosugi Y, Matsumoto K, Lytras S, Plianchaisuk A, Tolentino JE, Fujita S, Yo MS, Luo C, Kim Y, Shihoya W, Ito J, Nureki O, Sato K (2025) Molecular basis of sarbecovirus evolution and receptor tropism in natural hosts, potential intermediate hosts, and humans. *bioRxiv*

Lee J, Zepeda SK, Park YJ, Taylor AL, Quispe J, Stewart C, Leaf EM, Treichel C, Corti D, King NP, Starr TN, Veesler D (2023) Broad receptor tropism and immunogenicity of a clade 3 sarbecovirus. *Cell Host Microbe* 31: 1961-1973 e11

Li F (2008) Structural analysis of major species barriers between humans and palm civets for severe acute respiratory syndrome coronavirus infections. *J Virol* 82: 6984-91

Li F, Li W, Farzan M, Harrison SC (2005a) Structure of SARS coronavirus spike receptor-binding domain complexed with receptor. *Science* 309: 1864-8

Li W, Shi Z, Yu M, Ren W, Smith C, Epstein JH, Wang H, Crameri G, Hu Z, Zhang H, Zhang J, McEachern J, Field H, Daszak P, Eaton BT, Zhang S, Wang LF (2005b) Bats are natural reservoirs of SARS-like coronaviruses. *Science* 310: 676-9

Li W, Zhang C, Sui J, Kuhn JH, Moore MJ, Luo S, Wong SK, Huang IC, Xu K, Vasilieva N, Murakami A, He Y, Marasco WA, Guan Y, Choe H, Farzan M (2005c) Receptor and viral determinants of SARS-coronavirus adaptation to human ACE2. *EMBO J* 24: 1634-43

Liu B, Niu X, Deng Y, Zhang Z, Wang Y, Gao X, Liang H, Li Z, Wang Q, Cheng Y, Chen Q, Huang S, Pan Y, Su M, Lin X, Niu C, Chen Y, Yang W, Zhang Y, Yan Q et al. (2024) An unconventional VH1-2 antibody tolerates escape mutations and shows an antigenic hotspot on SARS-CoV-2 spike. *Cell Rep* 43: 114265

Ma J, Su D, Sun Y, Huang X, Liang Y, Fang L, Ma Y, Li W, Liang P, Zheng S (2021) Cryo-electron Microscopy Structure of S-Trimer, a Subunit Vaccine Candidate for COVID-19. *J Virol* 95: 10.1128/jvi.00194-21

Ma Y, Li P, Hu Y, Qiu T, Wang L, Lu H, Lv K, Xu M, Zhuang J, Liu X, He S, He B, Liu S, Liu L, Wang Y, Yue X, Zhai Y, Luo W, Mai H, Kuang Y et al. (2023) Spike substitution T813S increases Sarbecovirus fusogenicity by enhancing the usage of TMPRSS2. *PLOS Pathogens* 19: e1011123

Markotter W, Geldenhuys M, Jansen van Vuren P, Kemp A, Mortlock M, Mudakikwa A, Nel L, Nziza J, Paweska J, Weyer J (2019) Paramyxo- and Coronaviruses in Rwandan Bats. *Trop Med Infect Dis* 4: 99

McCallum M, De Marco A, Lempp FA, Tortorici MA, Pinto D, Walls AC, Beltramello M, Chen A, Liu Z, Zatta F, Zepeda S, di Iulio J, Bowen JE, Montiel-Ruiz M, Zhou J, Rosen LE, Bianchi S, Guarino B, Fregni CS, Abdelnabi R et al. (2021) N-terminal domain antigenic mapping reveals a site of vulnerability for SARS-CoV-2. *Cell* 184: 2332-2347 e16

Murakami S, Kitamura T, Suzuki J, Sato R, Aoi T, Fujii M, Matsugo H, Kamiki H, Ishida H, Takenaka-Uema A, Shimojima M, Horimoto T (2020) Detection and Characterization of Bat Sarbecovirus Phylogenetically Related to SARS-CoV-2, Japan. *Emerg Infect Dis* 26: 3025-3029

Ou X, Xu G, Li P, Liu Y, Zan F, Liu P, Hu J, Lu X, Dong S, Zhou Y, Mu Z, Wu Z, Wang J, Jin Q, Liu P, Lu J, Wang X, Qian Z (2023) Host susceptibility and structural and immunological insight of S proteins of two SARS-CoV-2 closely related bat coronaviruses. *Cell Discov* 9: 78

Park YJ, Liu C, Lee J, Brown JT, Ma CB, Liu P, Gen R, Xiong Q, Zepeda SK, Stewart C, Addetia A, Craig CJ, Tortorici MA, Alshukairi AN, Starr TN, Yan H, Veesler D (2025) Molecular basis of convergent evolution of ACE2 receptor utilization among HKU5 coronaviruses. *Cell* 188: 1711-1728 e21

Peiris JS, Chu CM, Cheng VC, Chan KS, Hung IF, Poon LL, Law KI, Tang BS, Hon TY, Chan CS, Chan KH, Ng JS, Zheng BJ, Ng WL, Lai RW, Guan Y, Yuen KY, Group HUSS (2003) Clinical progression and viral load in a community outbreak of coronavirus-associated SARS pneumonia: a prospective study. *Lancet* 361: 1767-72

Peiris JS, Guan Y, Yuen KY (2004) Severe acute respiratory syndrome. *Nat Med* 10: S88-97

Pettersen EF, Goddard TD, Huang CC, Couch GS, Greenblatt DM, Meng EC, Ferrin TE (2004) UCSF Chimera--a visualization system for exploratory research and analysis. *J Comput Chem* 25: 1605-12

Punjani A, Rubinstein JL, Fleet DJ, Brubaker MA (2017) cryoSPARC: algorithms for rapid unsupervised cryo-EM structure determination. *Nat Methods* 14: 290-296

Qu K, Chen Q, Ciazynska KA, Liu B, Zhang X, Wang J, He Y, Guan J, He J, Liu T, Zhang X, Carter AP, Xiong X, Briggs JAG (2022) Engineered disulfide reveals structural dynamics of locked SARS-CoV-2 spike. *PLoS Pathog* 18: e1010583

Rosa A, Pye VE, Graham C, Muir L, Seow J, Ng KW, Cook NJ, Rees-Spear C, Parker E, Dos Santos MS, Rosadas C, Susana A, Rhys H, Nans A, Masino L, Roustan C, Christodoulou E, Ulferts R, Wrobel AG, Short CE et al. (2021) SARS-CoV-2 can recruit a heme metabolite to evade antibody immunity. *Sci Adv* 7: eabg7607

Shuai H, Chan JF, Yuen TT, Yoon C, Hu JC, Wen L, Hu B, Yang D, Wang Y, Hou Y, Huang X, Chai Y, Chan CC, Poon VK, Lu L, Zhang RQ, Chan WM, Ip JD, Chu AW, Hu YF et al. (2021) Emerging SARS-CoV-2 variants expand species tropism to murines. *EBioMedicine* 73: 103643

Si JY, Chen YM, Sun YH, Gu MX, Huang ML, Shi LL, Yu X, Yang X, Xiong Q, Ma CB, Liu P, Shi ZL, Yan H (2024) Sarbecovirus RBD indels and specific residues dictating multi-species ACE2 adaptiveness. *Nat Commun* 15: 8869

Song W, Gui M, Wang X, Xiang Y (2018) Cryo-EM structure of the SARS coronavirus spike glycoprotein in complex with its host cell receptor ACE2. *PLoS Pathog* 14: e1007236

Tan CCS, Trew J, Peacock TP, Mok KY, Hart C, Lau K, Ni D, Orme CDL, Ransome E, Pearse WD, Coleman CM, Bailey D, Thakur N, Quantrill JL, Sukhova K, Richard D, Kahane L, Woodward G, Bell T, Worledge L et al. (2023) Genomic screening of 16 UK native bat species through conservationist networks uncovers coronaviruses with zoonotic potential. *Nat Commun* 14: 3322

Tao Y, Tong S (2019) Complete Genome Sequence of a Severe Acute Respiratory Syndrome-Related Coronavirus from Kenyan Bats. *Microbiol Resour Announc* 8

Temmam S, Vongphayloth K, Baquero E, Munier S, Bonomi M, Regnault B, Douangboubpha B, Karami Y, Chretien D, Sanamxay D, Xayaphet V, Paphaphanh P, Lacoste V, Somlor S, Lakeomany K, Phommavanh N, Perot P, Dehan O, Amara F, Donati F et al. (2022) Bat coronaviruses related to SARS-CoV-2 and infectious for human cells. *Nature* 604: 330-336

Toelzer C, Gupta K, Yadav SKN, Borucu U, Davidson AD, Kavanagh Williamson M, Shoemark DK, Garzoni F, Staufer O, Milligan R, Capin J, Mulholland AJ, Spatz J, Fitzgerald D, Berger I, Schaffitzel C (2020) Free fatty acid binding pocket in the locked structure of SARS-CoV-2 spike protein. *Science* 370: 725-730

Wacharapluesadee S, Tan CW, Maneeorn P, Duengkae P, Zhu F, Joyjinda Y, Kaewpom T, Chia WN, Ampoot W, Lim BL, Worachotsueptrakun K, Chen VC, Sirichan N, Ruchisrisarod C, Rodpan A, Noradechanon K, Phaichana T, Jantarat N, Thongnumchaima B, Tu C et al. (2021) Evidence for SARS-CoV-2 related coronaviruses circulating in bats and pangolins in Southeast Asia. *Nat Commun* 12: 972

Wang J, Ma Y, Li Z, Yuan H, Liu B, Li Z, Su M, Habib G, Liu Y, Fu L, Wang P, Li M, He J, Chen J, Zhou P, Shi Z, Chen X, Xiong X (2025) SARS-related coronavirus S-protein structures reveal synergistic RBM interactions underpinning high-affinity human ACE2 binding. *Sci Adv* 11: eadr8772

Wells HL, Letko M, Lasso G, Ssebide B, Nziza J, Byarugaba DK, Navarrete-Macias I, Liang E, Cranfield M, Han BA, Tingley MW, Diuk-Wasser M, Goldstein T, Johnson CK, Mazet JAK, Chandran K, Munster VJ, Gilardi K, Anthony SJ (2021) The evolutionary history of ACE2 usage within the coronavirus subgenus Sarbecovirus. *Virus Evol* 7: veab007

Xiong X, Qu K, Ciazynska KA, Hosmillo M, Carter AP, Ebrahimi S, Ke Z, Scheres SHW, Bergamaschi L, Grice GL, Zhang Y, Collaboration C-NC-B, Nathan JA, Baker S, James LC, Baxendale HE, Goodfellow I, Doffinger R, Briggs JAG (2020) A thermostable, closed SARS-CoV-2 spike protein trimer. *Nat Struct Mol Biol* 27: 934-941

Yan Q, Gao X, Liu B, Hou R, He P, Ma Y, Zhang Y, Zhang Y, Li Z, Chen Q, Wang J, Huang X, Liang H, Zheng H, Yao Y, Chen X, Niu X, He J, Chen L, Zhao J et al. (2024)

Antibodies utilizing VL6-57 light chains target a convergent cryptic epitope on SARS-CoV-2 spike protein and potentially drive the genesis of Omicron variants. *Nat Commun* 15: 7585

Yan R, Zhang Y, Li Y, Xia L, Guo Y, Zhou Q (2020) Structural basis for the recognition of SARS-CoV-2 by full-length human ACE2. *Science* 367: 1444-1448

Yu H, Liu B, Zhang Y, Gao X, Wang Q, Xiang H, Peng X, Xie C, Wang Y, Hu P, Shi J, Shi Q, Zheng P, Feng C, Tang G, Liu X, Guo L, Lin X, Li J, Liu C et al. (2023) Somatically hypermutated antibodies isolated from SARS-CoV-2 Delta infected patients cross-neutralize heterologous variants. *Nat Commun* 14: 1058

Zhang J, Xiao T, Cai Y, Chen B (2021a) Structure of SARS-CoV-2 spike protein. *Curr Opin Virol* 50: 173-182

Zhang S, Qiao S, Yu J, Zeng J, Shan S, Tian L, Lan J, Zhang L, Wang X (2021b) Bat and pangolin coronavirus spike glycoprotein structures provide insights into SARS-CoV-2 evolution. *Nat Commun* 12: 1607

Zhang X, Li Z, Zhang Y, Liu Y, Wang J, Liu B, Chen Q, Wang Q, Fu L, Wang P, Zhong X, Jin L, Yan Q, Chen L, He J, Zhao J, Xiong X (2023) Disulfide stabilization reveals conserved dynamic features between SARS-CoV-1 and SARS-CoV-2 spikes. *Life Sci Alliance* 6: e202201796

Zhou H, Ji J, Chen X, Bi Y, Li J, Wang Q, Hu T, Song H, Zhao R, Chen Y, Cui M, Zhang Y, Hughes AC, Holmes EC, Shi W (2021) Identification of novel bat coronaviruses sheds light on the evolutionary origins of SARS-CoV-2 and related viruses. *Cell* 184: 4380-4391 e14

Zhou P, Yang XL, Wang XG, Hu B, Zhang L, Zhang W, Si HR, Zhu Y, Li B, Huang CL, Chen HD, Chen J, Luo Y, Guo H, Jiang RD, Liu MQ, Chen Y, Shen XR, Wang X, Zheng XS et al. (2020a) A pneumonia outbreak associated with a new coronavirus of probable bat origin. *Nature* 579: 270-273

Zhou T, Tsybovsky Y, Gorman J, Rapp M, Cerutti G, Chuang GY, Katsamba PS, Sampson JM, Schon A, Bimela J, Boyington JC, Nazzari A, Olia AS, Shi W, Sastry M, Stephens T, Stuckey J, Teng IT, Wang P, Wang S et al. (2020b) Cryo-EM Structures of SARS-CoV-2 Spike without and with ACE2 Reveal a pH-Dependent Switch to Mediate Endosomal Positioning of Receptor-Binding Domains. *Cell Host Microbe* 28: 867-879 e5

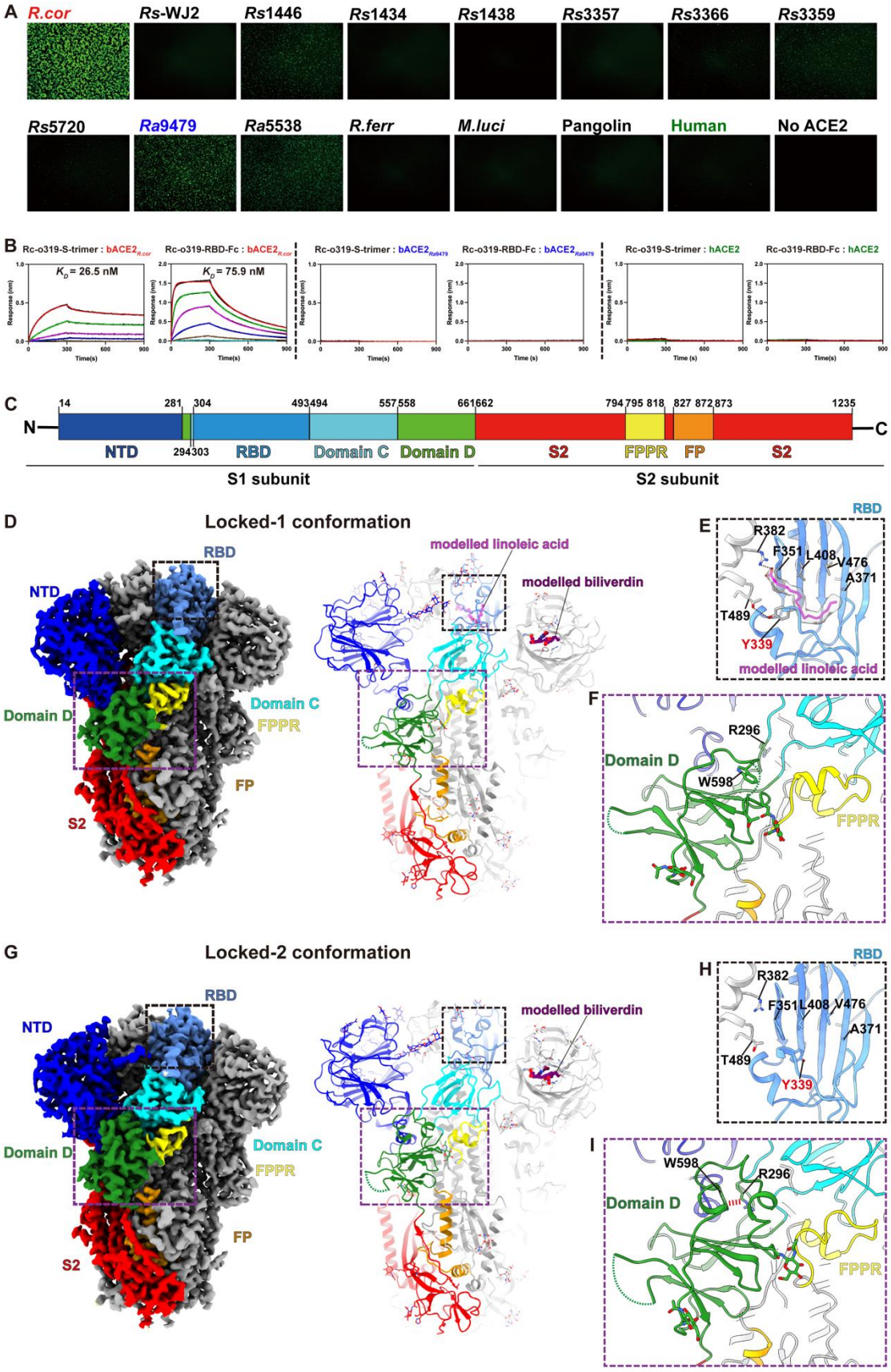
A
R.cor
Rs-WJ2
Rs1446
Rs1434
Rs1438
Rs3357
Rs3366
Rs3359
Rs5720
Ra9479
Ra5538
R.ferr
M.luci
Pangolin
Human
No ACE2
B
Rc-o319-S-trimer : bACE2R.cor
Rc-o319-RBD-Fc : bACE2R.cor
Rc-o319-S-trimer : bACE2Ra9479
Rc-o319-RBD-Fc : bACE2Ra9479
Rc-o319-S-trimer : hACE2
Rc-o319-RBD-Fc : hACE2
KD = 26.5 nM
KD = 75.9 nM
Response (nm)
Time(s)
C
N
C
14
281
304
493
494
557
558
661
662
794
795
818
827
872
873
1235
NTD
294
303
RBD
Domain C
Domain D
S2
FPPR
FP
S2
S1 subunit
S2 subunit
D
Locked-1 conformation
RBD
NTD
Domain D
Domain C
FPPR
FP
S2
modelled linoleic acid
modelled biliverdin
E
RBD
R382
F351
L408
V476
A371
T489
Y339
modelled linoleic acid
F
R296
Domain D
W598
FPPR
G
Locked-2 conformation
RBD
NTD
Domain D
Domain C
FPPR
FP
S2
modelled biliverdin
H
RBD
R382
F351
L408
V476
A371
T489
Y339
I
W598
R296
Domain D
FPPR

927

Figure 1. Rc-o319 S-protein utilizes a narrow range of *Rhinolophus* bat ACE2 orthologs as receptors and adopts two locked, 3-RBD-down conformations.

(A) Cell-cell fusion assays using receptor cells expressing bat, pangolin or human ACE2 molecules and effector cells expressing the Rc-o319 S-proteins. Fused cells show GFP signals. Representative images of cell-cell fusion captured at 6 hours post-transfection are shown. Scale bar, 500 μm. **(B)** Binding of Rc-o319 S-trimer to immobilized, dimeric bACE2$_{R.cor}$, hACE2 and bACE2$_{Ra9479}$ as assessed by BLI assays. **(C)** A schematic representation showing the eight functional domains or regions of Rc-o319 S-protein. **(D)** Cryo-EM density and associated molecular model showing the overall architecture of a Rc-o319 S-trimer in a locked-1 conformation. **(E)** Lipid binding pocket in the RBD of locked-1 Rc-o319 S-trimer. Modeled linoleic acid (magenta) interacts with the shown hydrophobic residues of the lipid binding pocket. Salt bridge and hydrogen bond are shown as dashed lines. **(F)** Structure of the Domain D region in the locked-1 Rc-o319 S-trimer. Consistent with a locked conformation, the fusion peptide proximal region (FPPR) is ordered. Residues 580-605$_{Rc\text{-}o319}$ form a large disordered loop in the locked-1 conformation. **(G)** Cryo-EM density and associated molecular model showing the overall architecture of a locked-2 Rc-o319 S-trimer. **(H)** The RBD lipid binding pocket is empty with Y339$_{Rc\text{-}o319}$ side-chain reorientated in the locked-2 conformation. **(I)** Residues 580-605$_{Rc\text{-}o319}$ refold and form an ordered structure. A stabilizing cation-π interaction (red dashed line) is formed between Domain D residue W598$_{Rc\text{-}o319}$ and Domain C-D junction residue R296$_{Rc\text{-}o319}$.

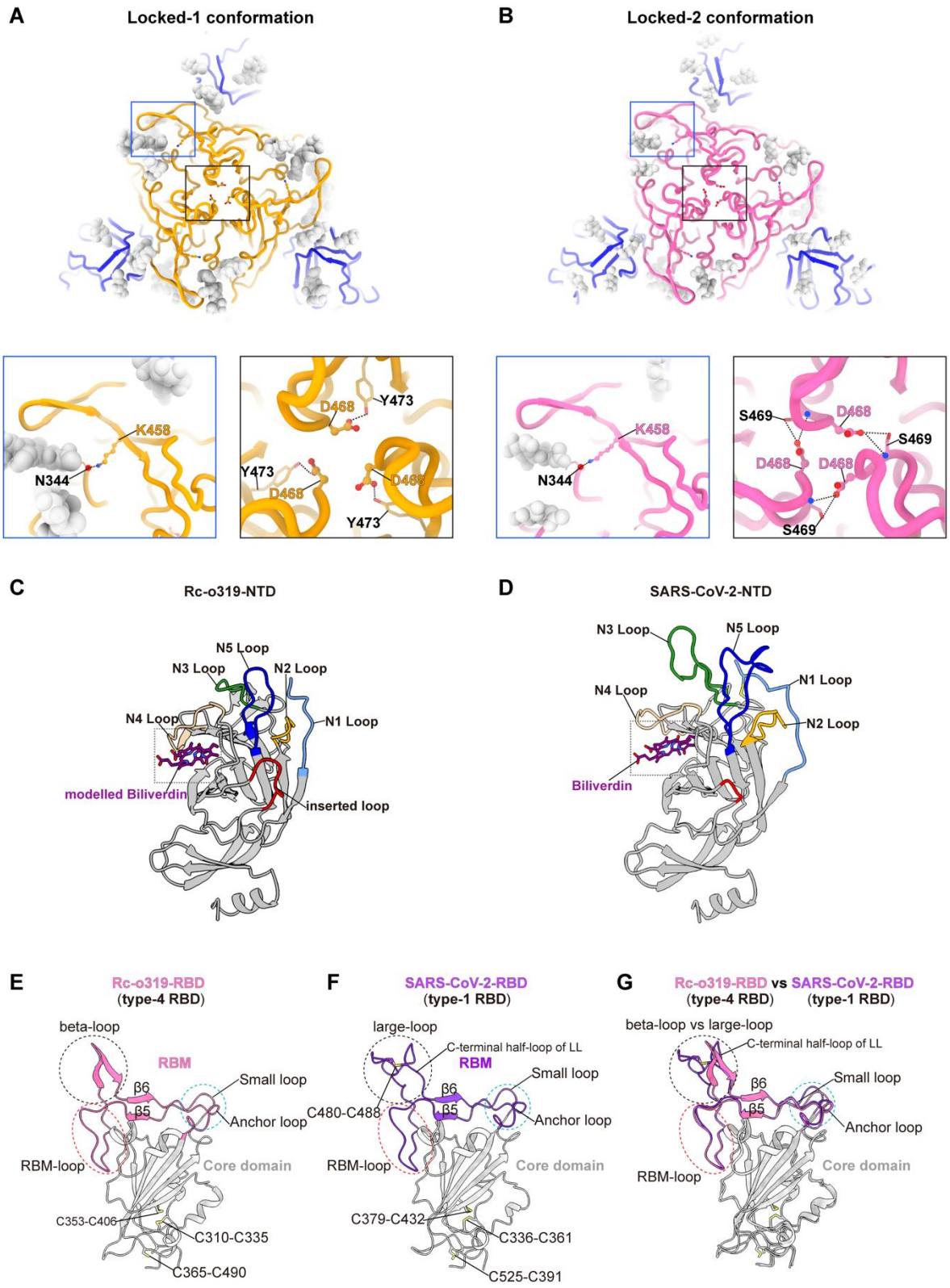
A
Locked-1 conformation
K458
N344
D468
Y473
Y473
D468
D468
Y473
B
Locked-2 conformation
K458
N344
S469
D468
S469
D468
D468
S469
C
Rc-o319-NTD
N5 Loop
N3 Loop
N2 Loop
N4 Loop
N1 Loop
modelled Biliverdin
inserted loop
D
SARS-CoV-2-NTD
N3 Loop
N5 Loop
N1 Loop
N4 Loop
N2 Loop
Biliverdin
E
Rc-o319-RBD
(type-4 RBD)
beta-loop
RBM
β6
β5
Small loop
Anchor loop
RBM-loop
Core domain
C353-C406
C310-C335
C365-C490
F
SARS-CoV-2-RBD
(type-1 RBD)
large-loop
C-terminal half-loop of LL
RBM
Small loop
β6
β5
C480-C488
Anchor loop
RBM-loop
Core domain
C379-C432
C336-C361
C525-C391
G
Rc-o319-RBD vs SARS-CoV-2-RBD
(type-4 RBD) (type-1 RBD)
beta-loop vs large-loop
C-terminal half-loop of LL
Small loop
β6
β5
Anchor loop
RBM-loop
Core domain

951

Figure 2. Rc-o319 S-trimer structures reveal an RBD featuring a novel RBM and an NTD with altered loops.

(A-B) Topviews of locked-1 and locked-2 Rc-o319 S-trimer structures. N-linked glycans are shown as light gray spheres. NTDs are colored blue, RBDs are colored orange (locked-1, A) or pink (locked-2, B). The lower panels show intra- or inter-protomer interactions involving RBD residues. $K458_{Rc\text{-}o319}$ forms an inter-protomer hydrogen bond with $N344_{Rc\text{-}o319}$ of an RBD of a neighboring protomer in both locked-1 and locked-2 S-trimers. In the locked-1 conformation, $D468_{Rc\text{-}o319}$ forms an intra-protomer hydrogen bond with $Y473_{Rc\text{-}o319}$; in the locked-2 conformation, $D468_{Rc\text{-}o319}$ instead mediates two inter-protomer hydrogen bonds with $S469_{Rc\text{-}o319}$ of an adjacent protomer. **(C-D)** Comparison of Rc-o319 (C) and SARS-CoV-2 (D) N-terminal domain (NTD) structures. The five highly variable NTD loops (N1-N5) are shown in the Rc-o319 and SARS-CoV-2 (PDB: 7XU4) NTD structures. A four-amino-acid residue insertion is highlighted in the Rc-o319 NTD in red. **(E)** The structure of the Rc-o319 RBD. The receptor binding motif (RBM) of the RBD is colored pink and the core of the RBD is colored gray. Disulfide bonds within the RBD are indicated. Featured structural elements, beta-Loop (BL), small loop (SL), Lamella (LM) sheets, β5 and β6, and the large RBM loop are indicated. **(E-G)** For comparison, the SARS-CoV-2 RBD (PDB:7XU4) is shown (F) and superposed on the Rc-o319 RBD structure (E).

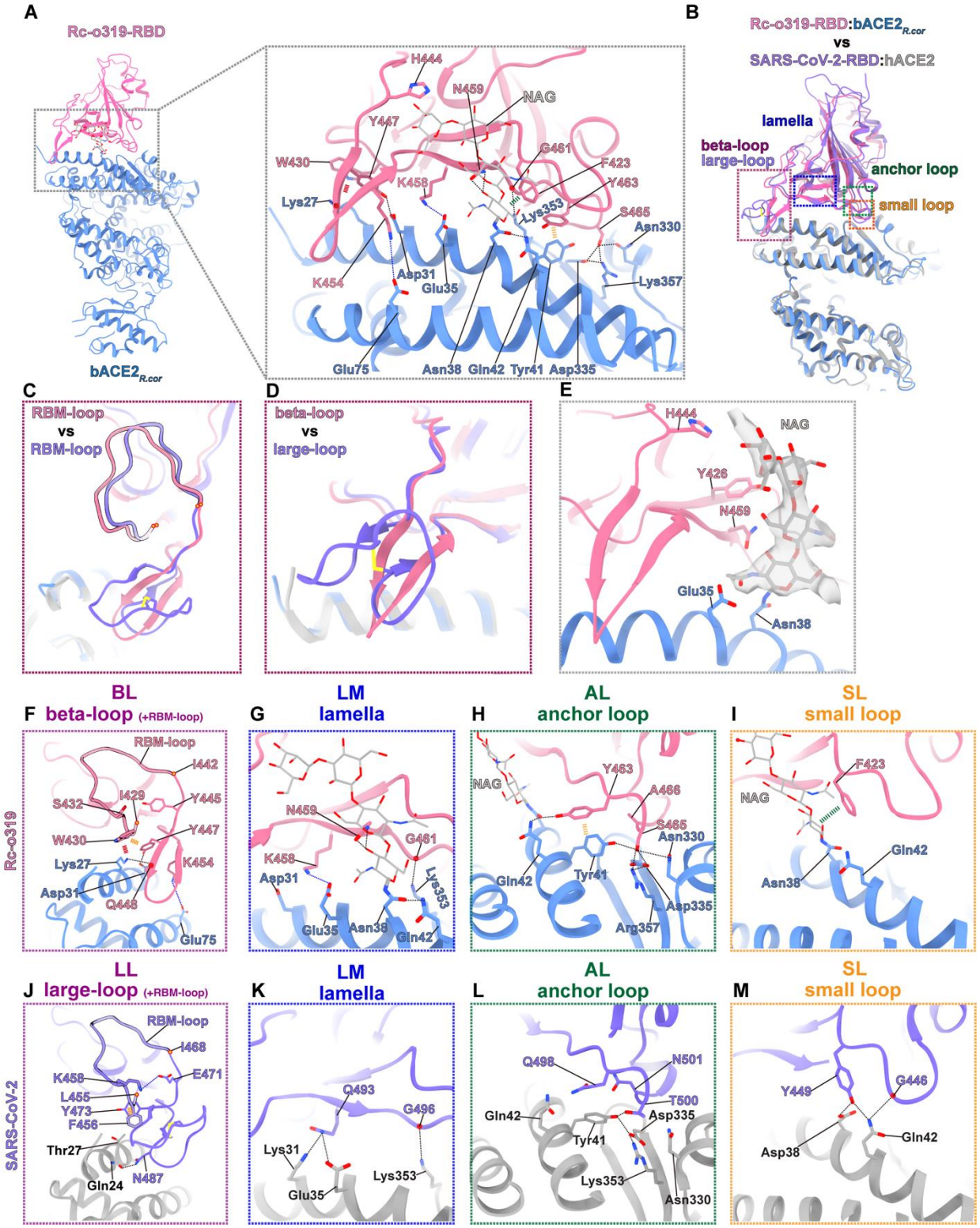

Figure 3. Cryo-EM structure of the Rc-o319-RBD:bACE2$_{R.cor}$ complex with a detailed comparison of RBD:ACE2 interactions versus those in the SARS-CoV-2-RBD:hACE2 complex.

(A) Molecular structure of a monomeric Rc-o319-RBD:bACE2$_{R.cor}$ complex extracted from the dimeric Rc-o319-RBD:bACE2$_{R.cor}$ complex structure resolved by cryo-EM (see Figure S1). Detailed interactions formed between the Rc-o319-RBD and bACE2$_{R.cor}$ are shown with hydrogen bonds and salt bridges shown as dashed lines. **(B)** Superposition of the Rc-o319-RBD:bACE2$_{R.cor}$ and SARS-CoV-2-RBD:hACE2 complex structures. The interface areas between the RBD and ACE2 in the two structures are divided into four regions: beta-loop (BL in Rc-o319-RBD)/large-loop (LL in SARS-CoV-2-RBD) (purple box), lamella (LM, blue box), anchor-loop (AL, green box), and small-loop (SL, orange box). **(C-D)** Comparison of the Rc-o319 RBM-loop and beta-loop (BL) with the RBM-loop and large-loop (LL) of SARS-CoV-2. **(E)** An N-linked glycan (shown in grey stick representation overlayed with white cryo-EM density) attached to Asn38 of bACE2$_{R.cor}$ is involved in the binding interface with Rc-o319-RBD, representing a unique structural feature. **(F-I)** Detailed interactions identified in the beta-loop+RBM-loop (BL, purple box), lamella (LM, blue box), anchor-loop (AL, green box), and small-loop (SL, orange box) regions of the interface between Rc-o319-RBD and bACE2$_{R.cor}$. **(J-M)** For comparison, detailed interactions are shown for the corresponding regions in the interface between SARS-CoV-2-RBD and hACE2. Hydrogen bonds, pi-pi (sugar-pi) interactions and cation-pi interactions are indicated by black, yellow (green) and red dashed lines, respectively.

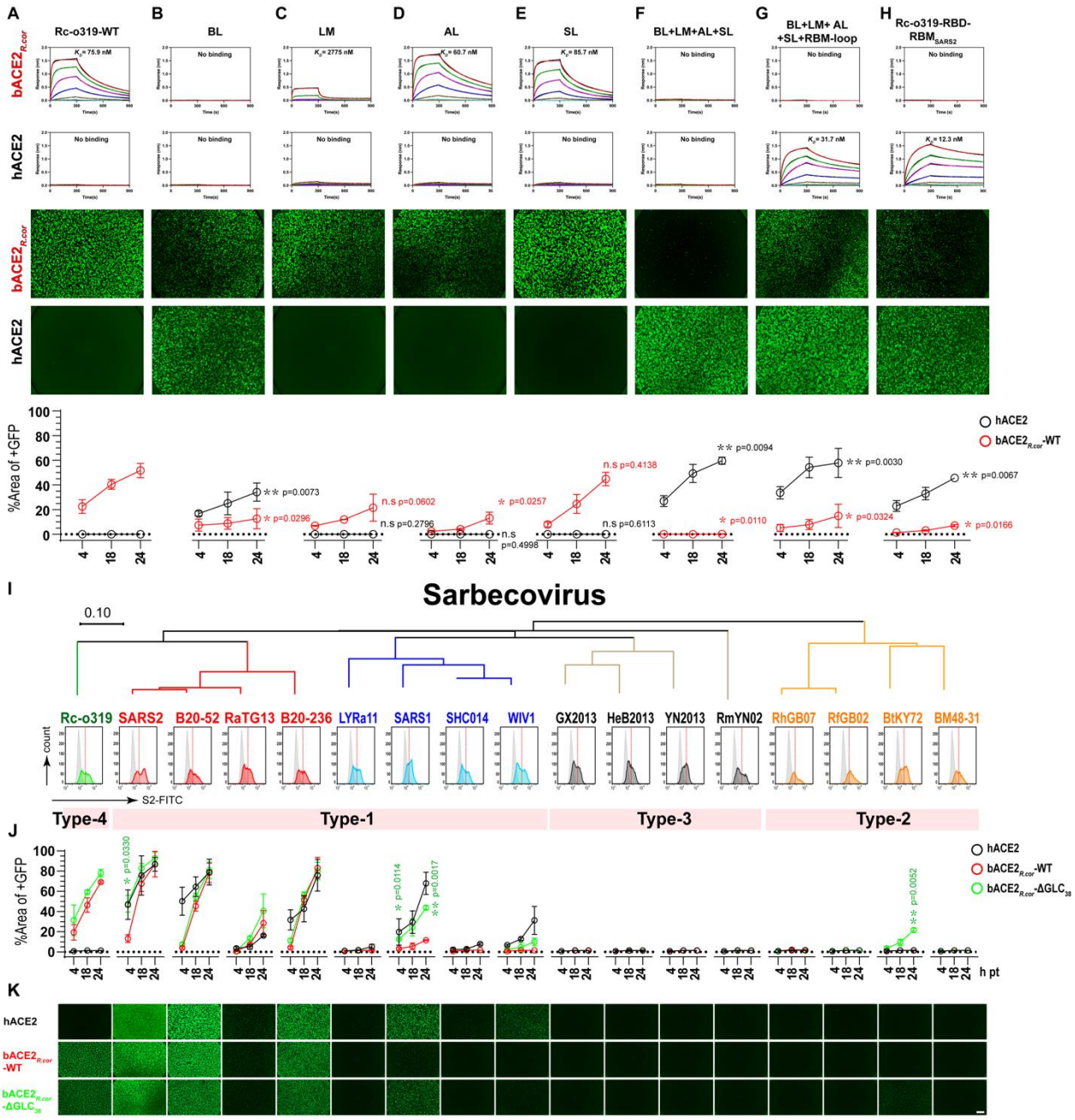

Figure 4. ACE2 utilization by wild-type and variant Rc-o319 S-proteins and bACE2$_{R.cor}$ utilization by different sarbecoviruses S-proteins.

(A-H) Top two panels, binding of bACE2$_{R.cor}$ and hACE2 by wild-type (WT) and variant Rc-o319-RBD-Fc proteins as assessed by BLI assays. Dimeric Rc-o319-RBD-Fc proteins were immobilized on the BLI sensors and tested binding against dimeric *Rhinolophus cornutus* bat ACE2 (bACE2$_{R.cor}$) or hACE2 protein as the analyte in solution. bACE2$_{R.cor}$ and hACE2 were three-fold serial diluted from 3000 to 4.1 nM. K_D values estimated from each binding experiment are shown

alongside the corresponding binding curves. Lower two panels, Representative images of cell-cell fusion captured at 12 hours post-transfection are shown. Scale bar, 500 μm. Effector cells expressing WT or variant Rc-o319 S-proteins were tested against receptor cells expressing either $bACE2_{R.cor}$ or hACE2. The bottom panels show the quantification of cell-cell fusion measuring the GFP+ area at 2, 6, 12 hours (h) post-transfection. Data are presented as mean ± s.d., n = 2. The *P* values were determined by unpaired t-test. $*P < 0.05$, $**P < 0.01$, $***P < 0.001$; NS, not significant. **(I)** Different sarbecovirus S-proteins are sorted based on S-protein phylogenetics and grouped by RBD types defined structurally. Type-1 strains are shown in red (SARS-CoV-2 clade) and blue (SARS-CoV-1 clade), type-2 strains in orange, type-3 strains in black and type-4 strains in green. Quantification of S-protein expression on the cell surface of effector cells by flow cytometry using an S2 antibody as the probe. Flow cytometry was repeated three times with representative data shown. **(J)** Effector cells shown in (**I**) were tested against receptor cells expressing hACE2 (gray line), $bACE2_{R.cor}$ (black line) and $bACE2_{R.cor}$-ΔGLC_{38} (green line, $bACE2_{R.cor}$ with the Thr40Ala mutation to remove the Asn38-glycan). Cell-cell fusion was quantified by assessing GFP+ areas (y-axis) at 4, 18, and 24 hours (h, x-axis) post-transfection (pt). Data are presented as mean ± s.d., n = 2. The *P* values were determined by unpaired t-test. $*P < 0.05$, $**P < 0.01$, $***P < 0.001$; NS, not significant. **(K)** Representative images of cell-cell fusion captured at 24 hours post-transfection are shown against receptor cells expressing different ACE2. Scale bar, 500 μm.

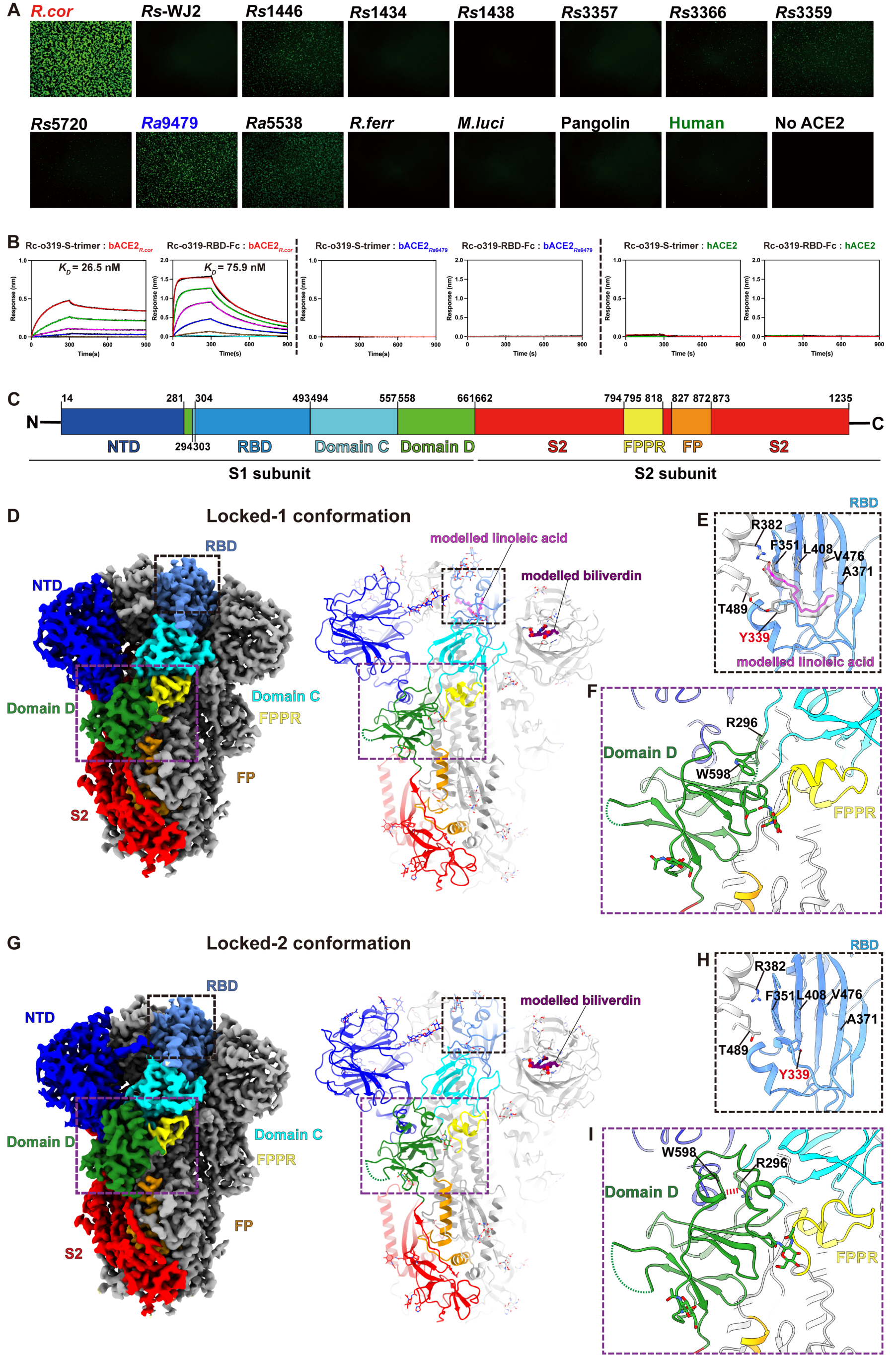
A
R.cor
Rs-WJ2
Rs1446
Rs1434
Rs1438
Rs3357
Rs3366
Rs3359
Rs5720
Ra9479
Ra5538
R.ferr
M.luci
Pangolin
Human
No ACE2
B
Rc-o319-S-trimer : bACE2R.cor
Rc-o319-RBD-Fc : bACE2R.cor
Rc-o319-S-trimer : bACE2Ra9479
Rc-o319-RBD-Fc : bACE2Ra9479
Rc-o319-S-trimer : hACE2
Rc-o319-RBD-Fc : hACE2
KD = 26.5 nM
KD = 75.9 nM
Response (nm)
Time(s)
C
N
C
14
281
304
493
494
557
558
661
662
794
795
818
827
872
873
1235
294
303
NTD
RBD
Domain C
Domain D
S2
FPPR
FP
S2
S1 subunit
S2 subunit
D
Locked-1 conformation
RBD
NTD
Domain D
Domain C
FPPR
FP
S2
modelled linoleic acid
modelled biliverdin
E
RBD
R382
F351
L408
V476
A371
T489
Y339
modelled linoleic acid
F
R296
Domain D
W598
FPPR
G
Locked-2 conformation
RBD
NTD
Domain D
Domain C
FPPR
FP
S2
modelled biliverdin
H
RBD
R382
F351
L408
V476
A371
T489
Y339
I
W598
R296
Domain D
FPPR

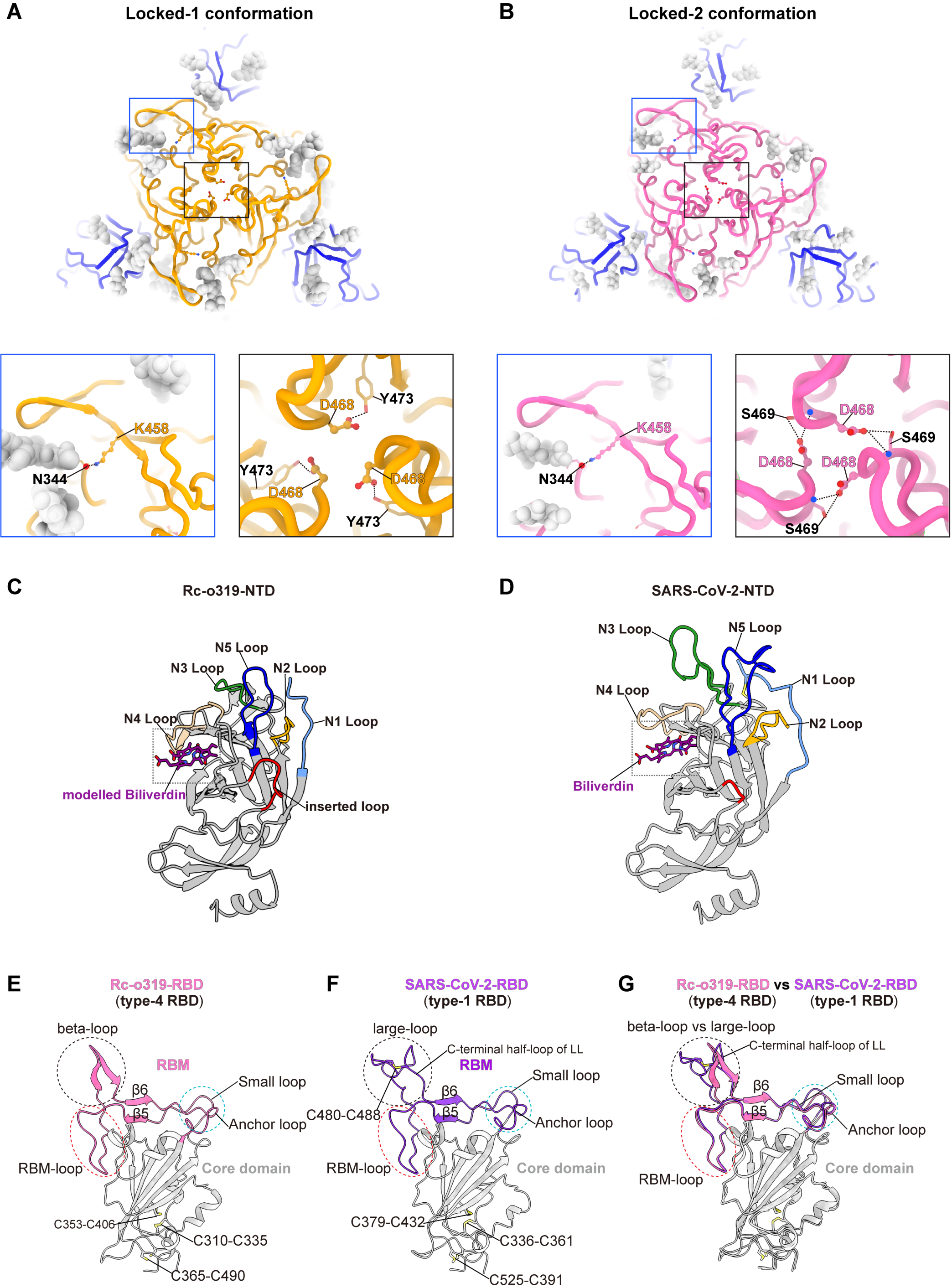
A
Locked-1 conformation
K458
N344
D468
Y473
Y473
D468
D468
Y473
B
Locked-2 conformation
K458
N344
S469
D468
S469
D468
D468
S469
C
Rc-o319-NTD
N5 Loop
N3 Loop
N2 Loop
N4 Loop
N1 Loop
modelled Biliverdin
inserted loop
D
SARS-CoV-2-NTD
N3 Loop
N5 Loop
N1 Loop
N4 Loop
N2 Loop
Biliverdin
E
Rc-o319-RBD
(type-4 RBD)
beta-loop
RBM
Small loop
β6
β5
Anchor loop
RBM-loop
Core domain
C353-C406
C310-C335
C365-C490
F
SARS-CoV-2-RBD
(type-1 RBD)
large-loop
C-terminal half-loop of LL
RBM
Small loop
β6
C480-C488
β5
Anchor loop
RBM-loop
Core domain
C379-C432
C336-C361
C525-C391
G
Rc-o319-RBD vs SARS-CoV-2-RBD
(type-4 RBD) (type-1 RBD)
beta-loop vs large-loop
C-terminal half-loop of LL
β6
Small loop
β5
Anchor loop
RBM-loop
Core domain

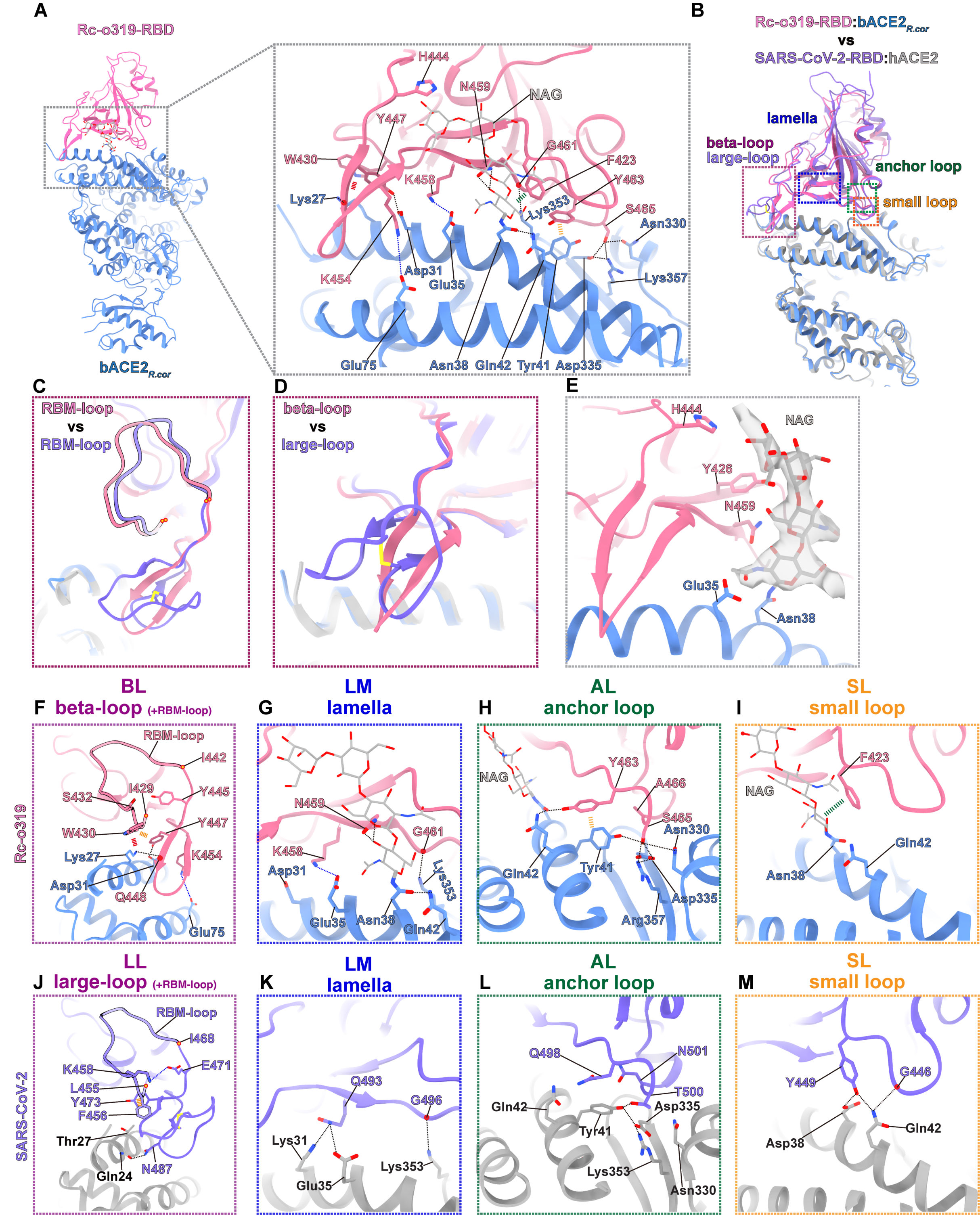
A
Rc-o319-RBD
bACE2R.cor
H444
N459
NAG
Y447
G461
W430
F423
K458
Y463
Lys27
Lys353
S465
Asn330
K454
Asp31
Glu35
Lys357
Glu75
Asn38
Gln42
Tyr41
Asp335
B
Rc-o319-RBD:bACE2R.cor
vs
SARS-CoV-2-RBD:hACE2
lamella
beta-loop
large-loop
anchor loop
small loop
C
RBM-loop
vs
RBM-loop
D
beta-loop
vs
large-loop
E
H444
NAG
Y426
N459
Glu35
Asn38
BL
F beta-loop (+RBM-loop)
LM
G lamella
AL
H anchor loop
SL
I small loop
Rc-o319
RBM-loop
I442
S432
I429
Y445
W430
Y447
Lys27
K454
Asp31
Q448
Glu75
N459
G461
K458
Asp31
Lys353
Glu35
Asn38
Gln42
NAG
Y463
A466
S465
Asn330
Gln42
Tyr41
Asp335
Arg357
F423
NAG
Gln42
Asn38
LL
J large-loop (+RBM-loop)
LM
K lamella
AL
L anchor loop
SL
M small loop
SARS-CoV-2
RBM-loop
I468
E471
K458
L455
Y473
F456
Thr27
Gln24
N487
Q493
G496
Lys31
Lys353
Glu35
Q498
N501
T500
Gln42
Asp335
Tyr41
Lys353
Asn330
Y449
G446
Gln42
Asp38

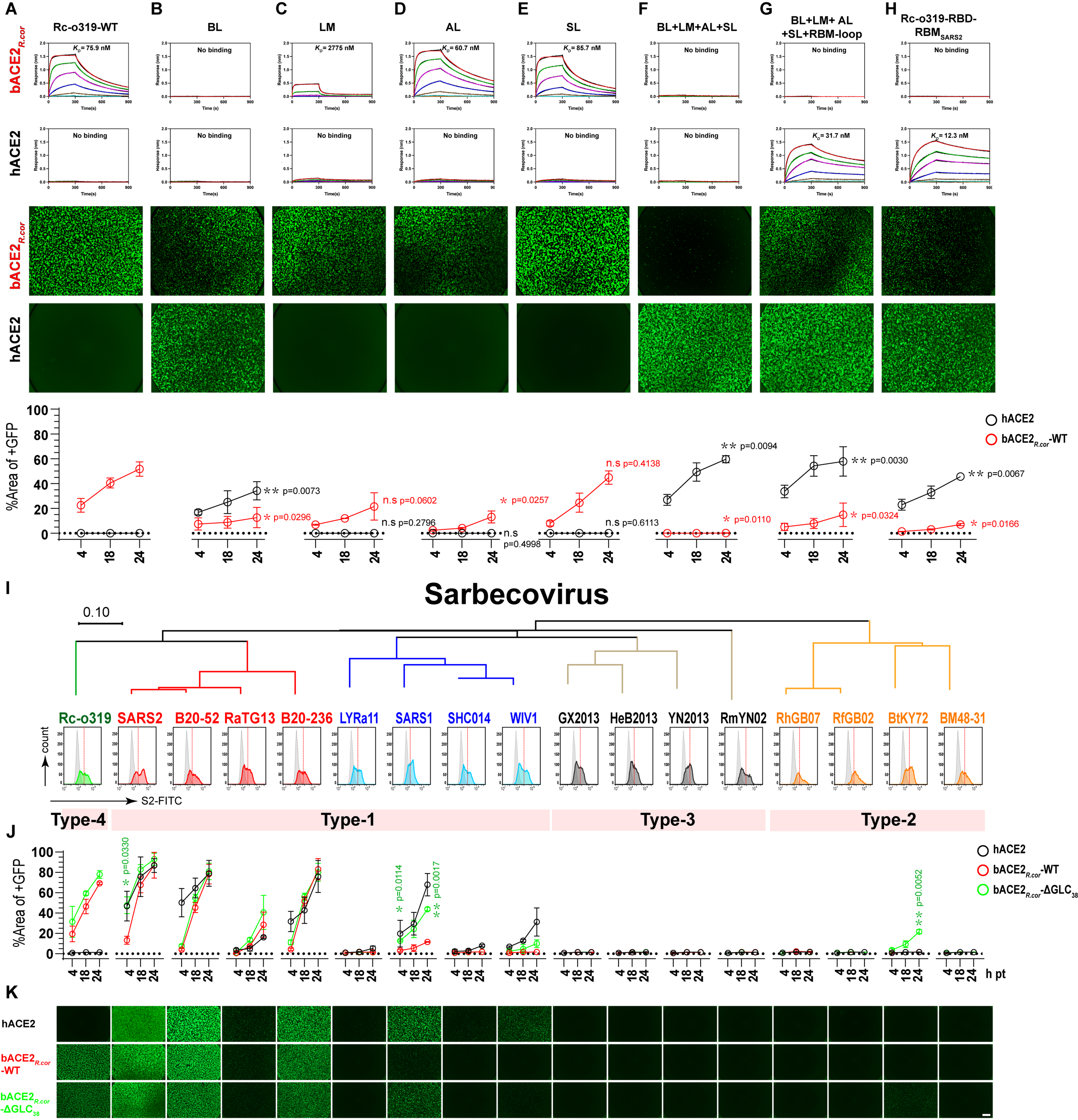
A
Rc-o319-WT
B
BL
C
LM
D
AL
E
SL
F
BL+LM+AL+SL
G
BL+LM+ AL +SL+RBM-loop
H
Rc-o319-RBD-RBM$_{SARS2}$
bACE2$_{R.cor}$
hACE2
K_D= 75.9 nM
No binding
K_D= 2775 nM
K_D= 60.7 nM
K_D= 85.7 nM
K_D= 31.7 nM
K_D= 12.3 nM
Response (nm)
Time(s)
%Area of +GFP
hACE2
bACE2$_{R.cor}$-WT
** p=0.0073
* p=0.0296
n.s p=0.0602
n.s p=0.2796
* p=0.0257
n.s p=0.4998
n.s p=0.4138
n.s p=0.6113
** p=0.0094
* p=0.0110
** p=0.0030
* p=0.0324
** p=0.0067
* p=0.0166
I
Sarbecovirus
0.10
Rc-o319 SARS2 B20-52 RaTG13 B20-236 LYRa11 SARS1 SHC014 WIV1 GX2013 HeB2013 YN2013 RmYN02 RhGB07 RfGB02 BtKY72 BM48-31
count
S2-FITC
Type-4
Type-1
Type-3
Type-2
J
%Area of +GFP
hACE2
bACE2$_{R.cor}$-WT
bACE2$_{R.cor}$-ΔGLC$_{38}$
* p=0.0330
* p=0.0114
** p=0.0017
** p=0.0052
h pt
K
hACE2
bACE2$_{R.cor}$-WT
bACE2$_{R.cor}$-ΔGLC$_{38}$